A consistent ocean oxygen profile dataset with new quality control and bias assessment

Viktor Gourteski[1,*], Lijing Cheng[1,*], Juan Du[1], Xiaogang Xing[2], Fei Chai[3,4], Zhetao Tan[1]

[1] Institute of Atmospheric Physics, Chinese Academy of Sciences, Beijing, China

[2] State Key Laboratory of Satellite Ocean Environment Dynamics, Second Institute of Oceanography, Ministry of Natural Resources, Hangzhou, China

[3] State Key Laboratory of Marine Environmental Science, Xiamen University, Xiamen, China

[4] College of Ocean and Earth Sciences, Xiamen University, Xiamen, China

Correspondence to: Viktor Gouretski (viktor.gouretski@posteo.de); Lijing Cheng (chenglij@mail.iap.ac.cn)

Abstract. The global ocean oxygen concentrations have declined in the past decades, posing threats to marine life and human society. High-quality and bias-free observations are crucial to understanding the ocean oxygen changes and assessing their impact. Here, we propose a new automated quality control (QC) procedure for ocean profile oxygen data. This procedure consists of a suite of ten quality checks, with outlier rejection thresholds being defined based on underlying statistics of the data. The procedure is applied to three main instrumentation types: bottle casts, CTD (Conductivity-Temperature-Depth) casts, and Argo profiling floats. Application of the quality control procedure to several manually quality-controlled datasets of good quality suggests the ability of the scheme to successfully identify outliers in the data. Collocated quality-controlled oxygen profiles obtained by means of the Winkler titration method are used as unbiased references to estimate possible residual biases in the oxygen sensor data. The residual bias is found to be negligible for electrochemical sensors typically used on CTD casts. We explain this as the consequence of adjusting to the concurrent sample Winkler data. Our analysis finds a prevailing negative residual bias for the delayed-mode quality-controlled and adjusted profiles from Argo floats varying from -4 to -1 μmol kg^{-1} among the data subsets adjusted by different Argo data assembly centers (DACs). The respective overall DAC-specific corrections are suggested. Applying the new QC procedure and bias adjustment resulted in a new global ocean oxygen dataset from 1920 to 2023 with consistent data quality across bottle samples, CTD casts, and Argo floats. The adjusted Argo profile data is available at the Marine Science Data Center of the Chinese Academy of Sciences (Gouretski et al., 2023, http://dx.doi.org/10.12157/IOCAS.20231208.001)

1 Introduction

Progressive warming caused by the human-induced increase of the greenhouse gases in the Earth's atmosphere leads to the decline of the dissolved oxygen concentration in the global ocean because of the reduction in oxygen solubility, the increase in stratification, which hampers the exchange between the surface layer and the ocean interior, and the accompanying change of ocean circulation (Keeling et al., 2010; Gruber et al., 2011; Deutsch et al., 2011; Praetorius et al., 2015; Oschlies et al., 2018). Another factor related to human activities is the increasing input of nutrients from agriculture and wastewater in the coastal regions (Oschlies et al., 2018; Breitburg et al., 2018). Nutrients facilitate the growth of phytoplankton and microbes subsequently decrease oxygen levels after the phytoplankton dies (Breitburg et al., 2018; Pitcher et al., 2021).

Recognizing the crucial role of dissolved oxygen for marine aerobic organisms, oceanographers started to measure oxygen in the late 19th century using the chemical method developed by Winkler

51 (1888). Since then, Winkler titration has been a standard method used on oceanographic ships and

52 in laboratories (Langdon, 2010), and the technique has an accuracy estimated to be 0.1% or ±0.3

53 μmol kg^{-1} (Carpenter, 1965).

54   With the rapid technological progress during the 1960-70s and the development of the

55 electronic CTD (Conductivity-Temperature-Depth) profilers, the first electrochemical sensors

56 appeared, providing the possibility for continuous oxygen profiling, which is not possible with the

57 Winkler method restricted by water samples from several depth levels. Electrochemical sensors are

58 based on a Clark polarographic membrane (Clark et al., 1953). Oxygen concentration outside the

59 membrane and oxygen diffusion through the membrane determine the sensor response.

60 Electrochemical Clark-type sensors possess a very fast time response (<1 s), with an initial accuracy

61 of 2% of oxygen saturation and precision of about 1 μmol kg^{-1} (Coppola et al., 2013). However,

62 sensor drift due to fouling and electrolyte consumption over time requires periodic calibration. The

63 first type of sensors applied on Biogeochemical Argo profiling floats (BGC floats) were Clark-type

64 electrodes (Riser and Johnson, 2008).

65   Optical oxygen sensors called "optodes" are based on the principle of fluorescence quenching

66 of a fluorescent indicator embedded in a sensing foil (Körtzinger et al., 2005, Tengberg et al., 2006).

67 The optode sensors appeared soon after the first implementation of the Clark-type sensors on Argo

68 floats (Gruber et al., 2010). Compared to electrochemical sensors, optodes are characterized by

69 long-term stability and high precision with the disadvantage of a slower response time (Gregoire et

70 al., 2021). During the initial period of several years, both Clarke-type and optode sensors were used

71 on Argo floats (Claustre et al., 2020). However, drift and initial calibration issues with

72 electrochemical sensors have led to the increased implementation of optodes on Argo floats

73 (Claustre et al., 2020), for which calibration using simultaneous water samples is not possible. From

74 the beginning of the BGC-Argo float implementation until March 2024, there have been more than

75 2100 Profiling biogeochemical (BGC) Argo floats that provide ocean oxygen observations with

76 unprecedented temporal and spatial resolutions in this century (Johnson et al. 2017; Roemmich et

77 al. 2019).

78   Different techniques have been applied in the past to collect ocean oxygen data, and the total

79 number of oxygen profile data from all instrument types within the World Ocean Database (Boyer

80 et al., 2018) reached a total of more than 1.2 million by 2023. However, there are a lot of data

81 quality issues in the historical oxygen database due to many reasons, including instrumental errors,

82 data collection failure, data processing errors, improper sample storage, unit conversion and others.

83 Furthermore, as different instruments have different data quality, merging several instrumentation

84 types into an integrated database requires proof of data consistency.

85   These quality issues impede the various applications of oxygen data, for instance, investigating

86   how much oxygen the ocean has lost in the past decades (Levin et al., 2018; Gregoire et al., 2021).

87   Previous assessments indicate the decline of open ocean full-depth O_2 content of 0.3%~2% since

88   the 1960s, with an upper 1000 m O_2 content decrease of 0.5–3.3% *(0.2–1.2 μmol kg^{-1} dec^{-1})* during

89   1970–2010 (Gulev et al. 2023). The maximum estimate is at least 6 times larger than the minimum

90   one, suggesting substantial uncertainty in quantifying the open ocean oxygen changes, which is a

91   grand challenge for the accurate assessment of deoxygenation (Helm et al. 2011; Long et al. 2016;

92   Ito et al. 2017; Schmidtko et al. 2017; Breitburg et al. 2018; Sharp et al. 2023). Furthermore, there

93   is a mismatch between observed and modelled trends in dissolved upper-ocean oxygen over the last

94   50 years (Stramma et al. 2012). Uncertainties and differences between estimates are at least partly

95   attributed to the oxygen data quality issues and inconsistency introduced by different instrument

96   types (e.g. different precision, instrument-specific errors/biases) (Gregoire et al., 2021). For

97   example, some BGC-Argo data conduct in-air oxygen measurements, which can be used to correct

98   potential systematic errors, while in other cases, a climatology is used (i.e. World Ocean Atlas) as a

99   reference (Bittig and Körtzinger, 2015; Gregoire et al., 2021). Therefore, a consistent and thorough

100 assessment of oxygen data quality, including uniform data quality control for all instruments and

101 instrumental bias assessments/corrections, is critical to providing a homogeneous ocean oxygen

102 database for various follow-on applications, including quantification of the trend of ocean

103 deoxygenation.

104   The paper aims to provide a quality-controlled (QC-ed), consistent global oxygen dataset for

105 the entire period 1920-2023. To achieve this goal, a novel automated QC procedure for ocean

106 oxygen profiles was developed. We implement this QC procedure in the global archive and analyze

107 and describe the quality of oxygen data obtained by different instrumentation types. The

108 performance of the quality control procedure is assessed using subsets of high-quality hydrographic

109 data and the QC-ed BGC Argo float profiles. Finally, we use bottle sample data obtained through

110 the Winkler method as a reference to assess oxygen biases for ship-based CTD and BGC Argo

111 oxygen profiles.

112   The rest of the paper is organized as follows. The data and methods employed in the study are

113 presented in Section 2. The data QC procedure is introduced in Section 3, with the data quality

114 assessment presented in Section 4. The results of benchmarking the automated QC procedure using

115 manually controlled datasets are shown in Section 5. Assessment of the residual bias for Argo and

116 CTD profiles is conducted in Section 6. The impacts of QC and bias adjustment on estimating

117 oxygen climatology and its changes (including annual cycle and long-term changes) are

120

2   Global archive of dissolved oxygen profiles

122   The original oxygen profile data at observed levels are sourced from two large depositories: 1)
123 World Ocean Database (WOD) (as of January 2023) and 2) oxygen profiles from the Argo Global
124 Data Assembly Center (GDAC) (ARGO, 2000). World Ocean Database (Boyer et al., 2018)
125 represents the largest depository of the dissolved oxygen profile data. For the current study, we used
126 ship-based WOD oxygen data coming from two main instrumentation types: 1) Ocean Station Data
127 (OSD) and 2) high-resolution CTD profiles. OSD instrumentation group is represented by bottle
128 casts with oxygen determined by the Winkler method. CTD profiles are obtained mainly through
129 the electrochemical sensors. For the Argo float data from GDACs, both raw (unadjusted) and
130 adjusted and QC-ed data are available with the latter used for the study.

131   The OSD profiles are most abundant between the 1960s to 2000s, CTD profiles between the
132 1990s to 2010s, and Argo profiles dominate after 2010 (**Fig. 1**). The geographical distribution of
133 oxygen profiles is inhomogeneous (**Fig. 2**), with OSD profiles exhibiting almost global coverage
134 compared to CTD and Argo, with dense sampling typical for the near-coastal areas and a sparser
135 sampling in the central parts of the oceans (**Fig. 2a**). The CTD profiles are most abundant in the
136 North Atlantic Ocean and are represented by a sparse net of transoceanic sections in the central
137 parts of the main ocean basins, leaving large data gaps, especially in the central regions of Pacific,
138 Indian, and Southern oceans (**Fig. 2b**). The total number of profiles from all three groups exceeds
139 1.2 million for the time period 1920 to 2023, so manual QC of the global oxygen dataset is nearly
140 impossible.
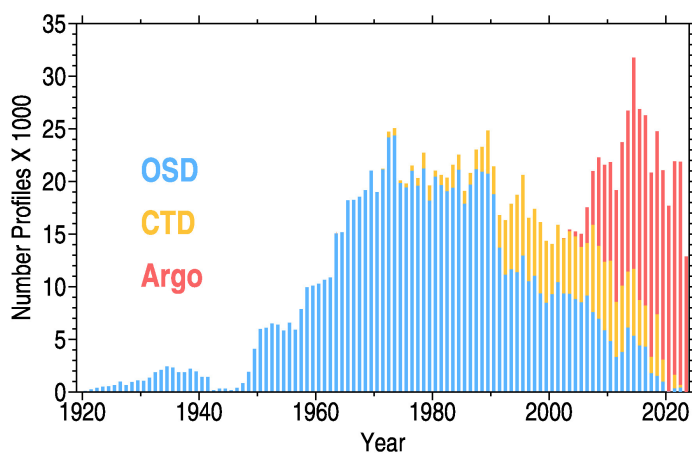
Figure 1. Yearly number of oxygen profiles from the World Ocean Database (OSD and CTD profiles) and national DACs (Argo) from 1920 to 2023.

141

142   Amounts of oxygen profiles disseminated by ten national Argo DACs and used for the current
143   study are given in Table 1. The most considerable contribution comes from two DACs: the Atlantic
144   Oceanographic and Meteorological Laboratory (AOML) and the French CORIOLIS Center
145   (Coriolis). Together, these two DACs contribute 71% of all oxygen profiles. The global sampling by
146   Argo floats is characterized by big gaps in the tropical belt of the World Ocean (**Fig. 2c**) and in the
147   marginal seas with shallow bottom depths.
148   The DACs report oxygen data along with quality flags set after the QC procedure performed by
149   each DAC. The spatial distribution of the profiles from each DAC is shown in **Fig. 3**. Only the
150   AOML dataset is characterized by a more or less global coverage. The profiles from the second
151   large Coriolis dataset are concentrated mostly in the Atlantic and Southern oceans. Other DACs are
152   characterized by a regional scope: Japan Meteorological Agency (JMA) data come from the Pacific
153   Ocean east of Japan, profiles from the Commonwealth Scientific and Industrial Research
154   Organization (CSIRO) cover the Southern Ocean, China Second Institute of Oceanography (CSIO)
155   mainly provides Argo profiles from the subtropical and tropical western Pacific Ocean, Argo
156   profiles from the British Oceanographic Data Centre (BODC) are located in the Atlantic Ocean.
157   Profiles from the Korea Ocean Research and Development Institute (KORDI) and from Korea
158   Meteorological Administration (KMA), the smallest two datasets, are located in the southern part of
159   the Sea of Japan.
160

161   **3   Data quality control**

162   Quality evaluation of hydrographic data typically consists of two parts: data QC for random
163   errors and evaluation of systematic errors or biases. These two issues are often treated separately
164   but represent the entire QC procedure. A unified QC procedure has yet to be suggested for the
165   global archive of oxygen profile data, and oxygen-related studies often rely on WOD (Garcia et al.,
166   2018), Argo (Thierry et al., 2021) and Bushnell et al. (2015) QC procedures. The efforts undertaken
167   under the International Quality-Controlled Ocean Database (IQuOD) initiative (Cowley, 2021)
168   resulted in a comprehensive study where different quality control procedures for temperature
169   profiles were compared and evaluated (Good et al., 2022). As shown in the previous section, the

170 characteristic feature of the global oxygen data archive is its heterogeneity. In the early years, a

171 relatively small amount of data permitted expert quality control, but for the actual global archive,

172 automated quality control procedures (AutoQC) are required.
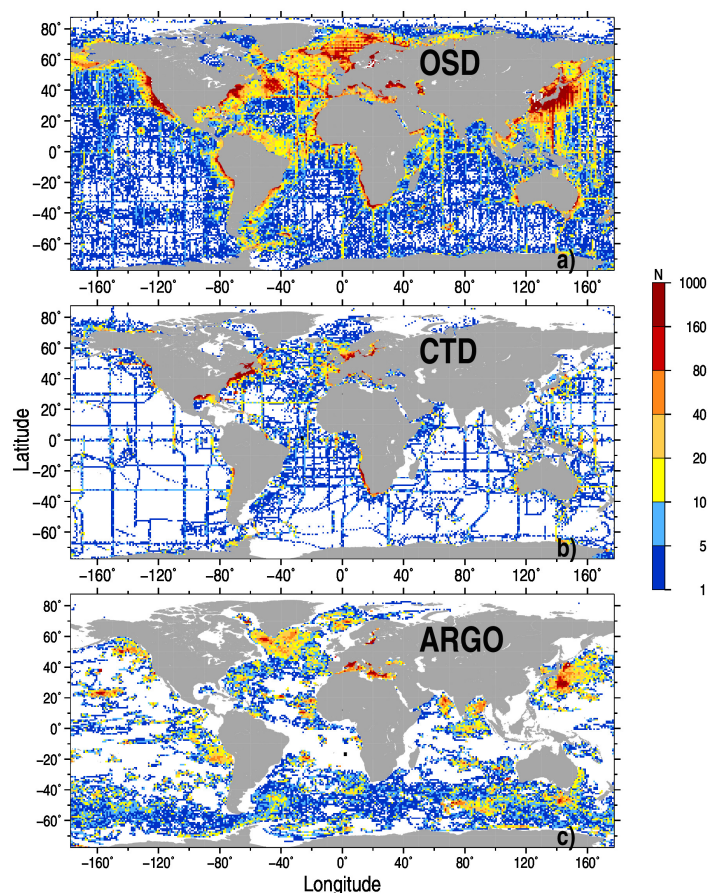
Figure 2. Number of profiles (N) in 1°×1° latitude/longitude squares for OSD (a), CTD (b), and Argo (c) data.

173

174   The AutoQC procedure aims to identify and flag outliers, which represent observations

175 significantly deviating from the majority of other data in the population. Monhor and Takemoto

176 (2005) noted that there is no rigid mathematical definition of an outlier. The outliers do not

177 necessarily represent erroneous measurements and can occur due to the natural variability of the

178 measured variable. A QC procedure defines outliers using a set of thresholds, which are based on

179 physical laws (for instance, the maximum solubility of gases in the water) or have to be defined

180 based on the statistical properties of the data population.

181   In this paper, we introduce a novel QC procedure capable of conducting quality assessment of

182 data from different instrumentation types. The procedure is applied to the observed level data and

does not require additional quality checks for profiles interpolated at a predefined set of levels. This second level of QC is an attribute of the WOD QC system (Garcia et al., 2018). To increase the reliability in detecting erroneous data, a set of quality-checks is applied to each profile. The larger the number of failed distinct quality checks, the higher the probability that the flagged observation represents a data outlier. Based on the available QC schemes for oceanographic data (most of them were developed for temperature and/or salinity profiles), quality checks can be subdivided into the following groups:

Group-1. Check of location, date and bottom depth of the profile.

Group-2. Check of profile attributes (maximum sampled depth, number of levels, variables measured) specific to each instrumentation type.

Group-3. Range check, e.g., comparison of observations at each level against minimum/maximum value thresholds, which are set for the entire ocean or oceanic basin (global ranges) or for the particular location and depth.

Group-4. Check of the profile shape, which is characterized by the vertical gradient of the measured variable at observed levels, by the number of local extrema, and by the presence of spikes**.**

It should be noted that QC procedures often assume Gaussian distribution law, and outliers are defined in terms of multiple times the standard deviation from the mean value (Z-score method). For instance, the WOD standard deviation check is based on this assumption (Garcia et al., 2018; Boyer et al., 2018). However, distributions of oceanographic parameters are typically skewed, and the assumption of Gaussian distribution leads to false data rejection. Tukey (1977) introduced a so-called box-plot method, which makes no assumption about the distribution law and is often used for outlier detection. Hubert and Vandervieren (2008) developed the adjusted Tukey's boxplot method for skewed distribution with fences depending on skewness. Following this approach, Gouretski (2018) and Tan et al. (2023) applied QC checks, taking into account the skewness of temperature distribution. In the current study we use the Hubert and Vandervieren (2008) adjusted boxplot method as modified by Adil and Irshad (2015).

Table 1. Argo oxygen profiles from different national DACs.

N	National Data Assembly Center	Code Name	Number of Argo profiles	Number of Argo profiles	Percent of Argo profiles having

				collocated with Winkler profiles	collocations with Winkler profiles
1	Atlantic Oceanographic and Meteorological Laboratory, US	AOML	89059	32396	41.08
2	CORIOLIS data Center, France	Coriolis	63220	33233	65.09
3	Commonwealth Scientific and Industrial Research Organization, Australia	CSIRO	19183	3302	23.75
4	Japan Meteorological Agency, Japan	JMA	15981	11233	82.90
5	Indian National Centre for Ocean Information Services, India	INCOIS	9901	2069	33.09
6	Second Institute of Oceanography, Ministry of Natural Resources, China	CSIO	6455	3921	68.98
7	Marine Environmental Data Service, Canada	MEDS	4605	14.04	50.50
8	British Oceanographic Data Center, UK	BODC	3533	1905	61.57
9	Korea Ocean Research and Development Institute, Korea	KORDI	2239	0	0
10	Korea Meteorological Administration, Korea	KMA	93	0	0

213

214   Developing the QC procedure, consisting of a suite of distinct checks, we assume that oxygen
215 data obtained by the reference Winkler method are superior in quality compared to the sensor data.
216 As noted by Golterman (1983), the principle of the Winkler method has been unchanged since its
217 introduction, with the method still providing the most precise determination of dissolved oxygen.
218 There is a total of ten distinct quality checks, which are introduced in sections 3.1 to 3.9. The outlier
219 statistics are shown in the respective supplements (**Fig. S1-Fig. S10**), both for the year/depth bins
220 and within 2°×4° geographical boxes and for randomly selected oxygen profiles affected by the
221 respective check.

222

223
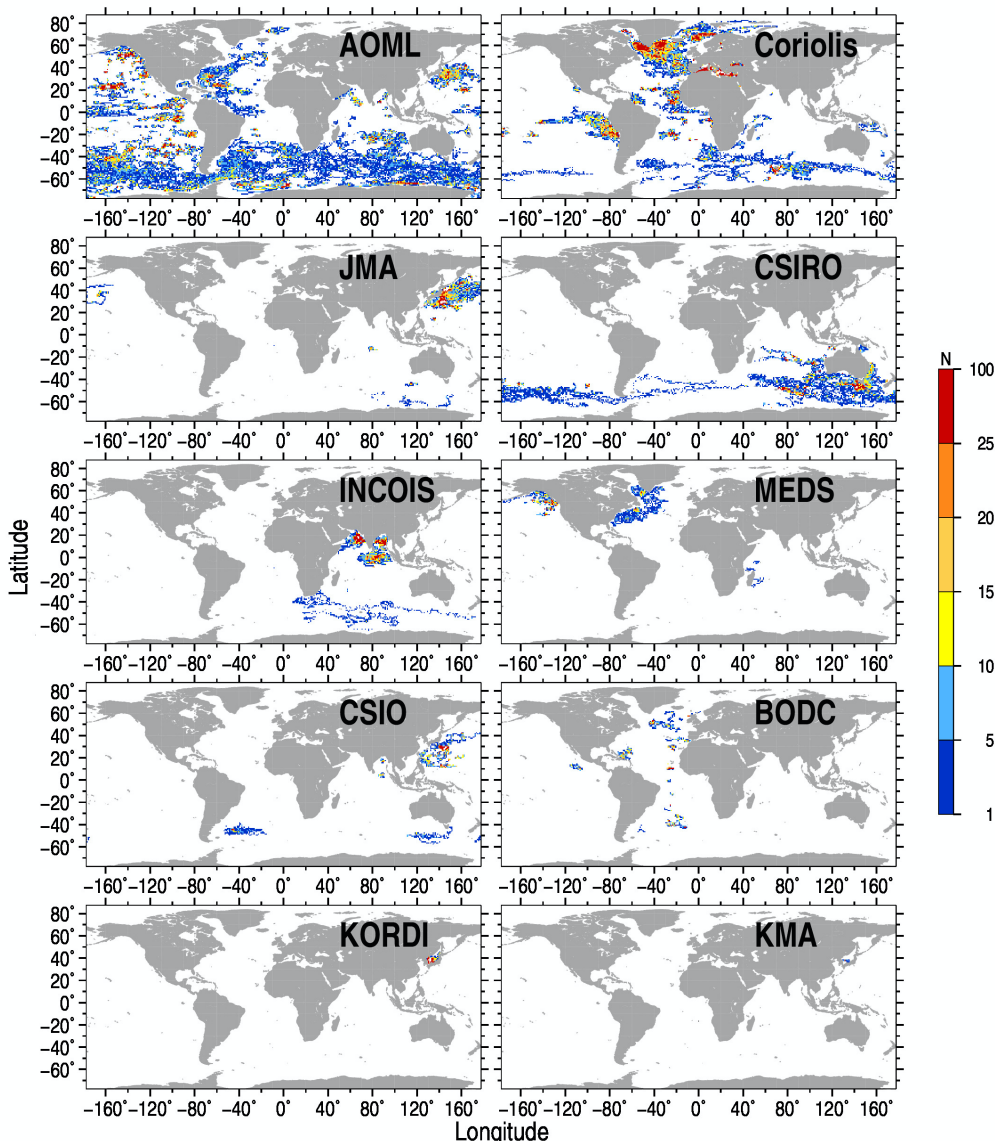
Figure 3. The number (N) of Argo oxygen profiles in 1°×1° spatial boxes for the datasets from different DACs. The name abbreviation of each DAC is also presented in each panel.

226

3.1 Geographical Location Check

A comparison of the deepest sampled level with the local ocean bottom depth may be used for the identification of erroneous geographical locations. We use GEBCO 0.5-minute resolution digital bathymetry map to define thresholds for this check. For each profile, the range between minimum and maximum GEBCO bottom depth within the 111 km radius is calculated. If the difference between the deepest profile measurement depth and the local GEBCO depth exceeds the above depth range, the geographical coordinates of the profile are considered to be in error and data at all

234 levels are flagged. According to Table 2, about 0.5% of OSD and CTD profiles fail this check,

235 compared to only 0.08% for Argo profiles. For each data type, the spatial distribution of profiles

236 failing this test exhibits a rather random pattern (**Fig. S1**). The highest percentage of OSD outlier

237 profiles are found for the time period before 1946, probably due to less accurate navigation methods

238 during the war (**Fig. S1b**). CTD profiles exhibit higher outlier scores above 400 m between 200-

239 2014 linked to several cruises. Only 0.077% of DAC QC-ed Argo profiles fail this check (**Fig. S1g-**

240 **i**).

241

242 **3.2   Global oxygen range check**

243   The test is applied to identify observations that are grossly in error (the so-called 'blunders').

244 These data correspond to the cases of the total instrumentation fault or crude errors introduced

245 during the data recording or formatting. The overall minimum/maximum oxygen ranges are defined

246 based on the entire archive of the OSD profiles. These overall ranges are set for depth levels and

247 temperature surfaces because the maximum oxygen solubility depends on temperature. For the

248 construction of overall limits, we use the normalized frequency histograms (**Fig. 4**). The

249 depth/oxygen histograms are constructed similarly with normalization at each depth level (**Fig. 4b**).

250 The normalization is done to account for varying numbers of oxygen observations with depth and

251 temperature. The relative frequencies serve as the guidance to produce the overall oxygen minimum

252 and maximum limits, which approximately correspond to the relative frequency of 0.05 (indicated

253 by the green lines). Spatial distribution of the OSD and CTD profiles with levels failing this check

254 broadly corresponds to the sampling density (**Fig. S2a, d and Fig. S3a, d**), whereas flagged Argo

255 profiles can be rather linked to distinct floats (**Fig. S2g, Fig. S3d**). The CTD data are characterized

256 by the largest fraction of profiles affected by this check (**Fig. S2e, Fig. S3e**).

257
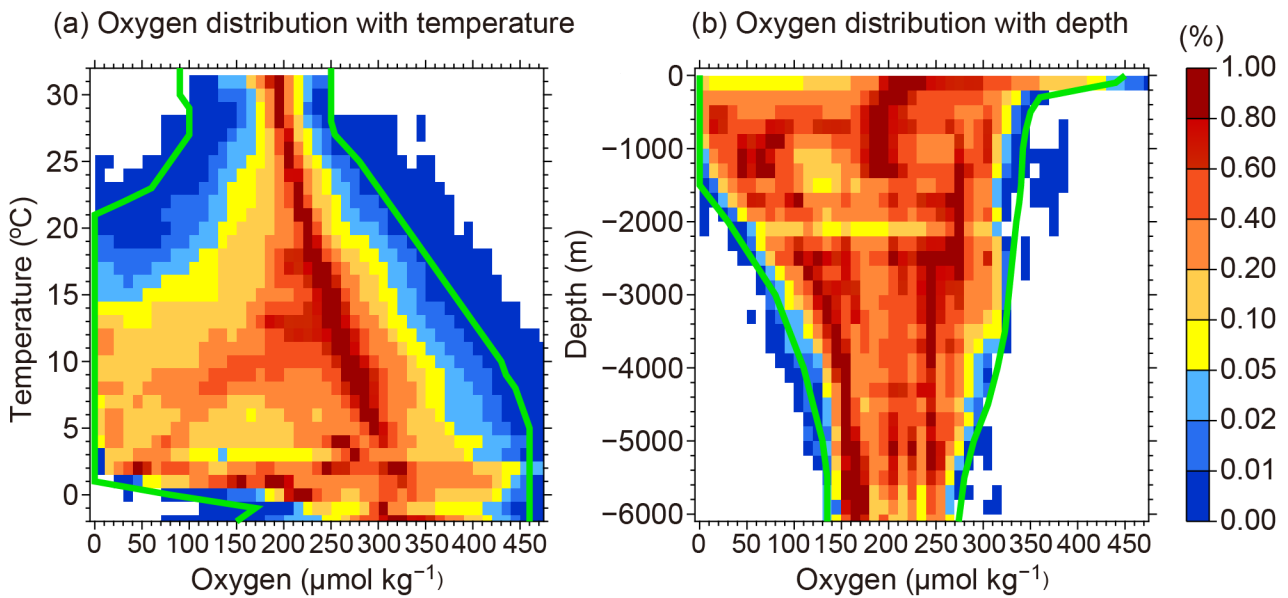
258

Figure 4. Normalized oxygen histograms used to define overall oxygen ranges versus temperature (a) and versus depth (b). Minimum and maximum overall oxygen limits are shown by solid green lines. For each temperature/oxygen bin in (a), the number of oxygen observations is divided by the number of observations in the most populated bin for the same temperature. The depth/oxygen histograms (b) are constructed similarly with normalization at each depth level.

259

3.3   Maximum oxygen solubility check

According to Henry's law, the quantity of an ideal gas that dissolves in a definite volume of liquid is directly proportional to the partial pressure of the gas. It is also known that gas solubility in the water typically decreases with increasing temperature. The histograms of observed oxygen concentration (C_{obs}) versus maximum oxygen solubility (C_{max}) calculated using reported temperature and salinity at different ocean layers depict a close relationship between the mode of observed oxygen distribution and the maximum solubility (**Fig. 5a-d**). The histograms also show that the distribution mode for the upper-most layer 0-100 m (**Fig. 5a**) follows the line $C_{obs} = C_{max}$ progressively deviating to lower C_{max} values when $C_{obs} > 300$ µmol kg^{-1}, suggesting an oxygen super-saturation. That is because in the photic layer of the ocean oxygen is produced by phytoplankton through photosynthesis, and oxygen super-saturation can evolve. Oxygen production due to photosynthesis leads to the formation of small bubbles (10-70 micron) with increasing oxygen super-saturation accompanied by a higher number of bubbles and their shift towards large sizes (Marks, 2008). In the deeper layers (**Fig. 5b-d**), the number of cases with super-saturation

274 decreases because of the reduced photosynthesis, so the temperature and pressure effects dominate.

275 According to the histograms (**Fig. 5a-d**), supersaturation is frequently observed in the upper layers.

276 The percentage of supersaturated values decreases from about 45 % in the near-surface layer to less

277 than 1.0 % below the 200 m level (**Fig. 5e, red**).

278
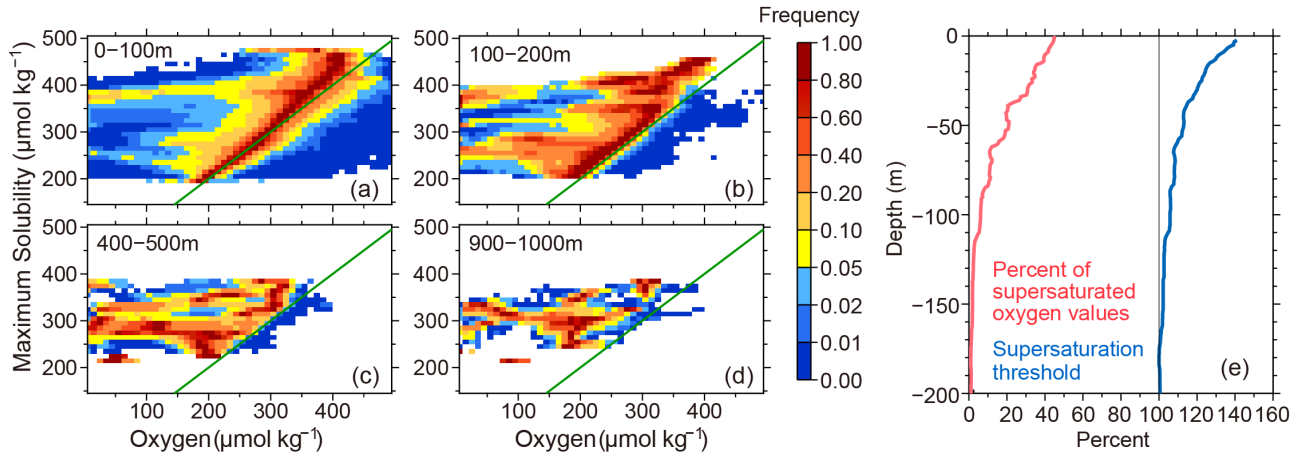
Figure 5. Super-saturation check: (a-d) normalized frequency histograms for maximum solubility versus reported dissolved oxygen value for different layers. The bin size is 10 μmol kg⁻¹. For each maximum solubility level, the frequencies for each bin are normalized by the number of the values in the most populated bin in order to account for variations in the number of profiles. (e) percentage of supersaturated oxygen values over all observed oxygen values (red) and the threshold for the super-saturation check, represented by the percentage relative to the maximum solubility (blue).

279

280   In order to set the threshold percentage for super-saturation, we calculated histograms of super-

281 saturation values for each 1-meter depth level of the upper 500 m layer. The threshold percentage of

282 super-saturation (**Fig. 5e**, blue line) corresponds to the 99th quantile. The threshold value

283 approaches 100% near the depth of 200m, therefore, below 200 m all supersaturated oxygen values

284 are flagged. Locations of profiles with at least one observed level failing this check are shown in

285 **Fig. S4a, d, g**. The distribution of profiles broadly corresponds to the spatial sampling density. The

286 OSD outliers are more numerous in the early years before 1955 probably pointing to less accurate

287 measurements during that time period. The check reveals a much higher percentage of CTD outliers

288 throughout the water column for several years before 2000 (**Fig. S4b**) compared to other

289 instrumentation types. Argo floats are characterized by the low outlier percentage for this quality

290 check with a higher percentage found for deep Argo floats between 2017-2018 below 2000m (**Fig.**
291 **S4h**).

292

293 **3.4   Stuck value check**

294   Malfunctioning of sensors often results in stuck values when the same oxygen concentration is
295 reported for all or most of the observed levels. To identify such profiles, we calculated oxygen
296 standard deviations for each oxygen profile to build histograms (**Fig. 6**) for each instrumentation
297 type. Only profiles with at least seven oxygen levels are considered. Unlike the OSD and Argo data,
298 for which the frequency of profiles drops for low standard deviation values, the CTD profiles are
299 characterized by a distinct peak for the lowest standard deviation values (**Fig. 6c**). Accordingly,
300 based on the histograms (**Fig. 6b, c**), we set the thresholds of 3 μmol kg^{-1} and 1 μmol kg^{-1} and for
301 CTD and Argo profiles, respectively. No lowest value thresholds are applied for OSD profiles, as
302 stuck values are only characteristics of the electronic sensors. The geographical distribution of
303 profiles failing this check is given in **Fig. S5 a, d**. The check is applied only to the CTD and Argo
304 sensor data and reveals a high percentage of outliers for CTD profiles, especially after 2000 (**Fig.**
305 **S5b**). Argo profiles which fail the check are not numerous and are located mostly in the Northern
306 Hemisphere (**Fig. S5d**).

307
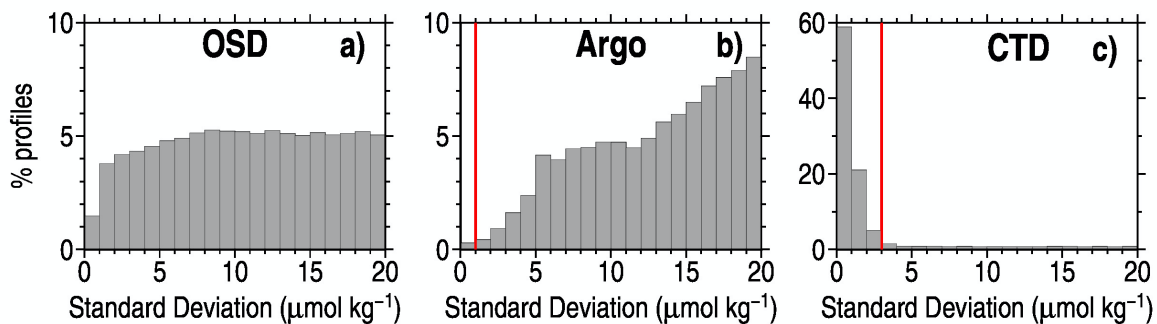
**Figure 6. Oxygen profile standard deviation for OSD (a), Argo (b), and CTD (c)
instrumentation types. Only profiles with at least seven levels of oxygen data are considered.
Red vertical lines show the respective threshold values for Argo and CTD profiles.**

308

309 **3.5   Multiple extrema check**

310   Multiple extrema check aims to identify profiles whose shape significantly deviates from the
311 majority of profiles. For each profile with at least 7 observed levels (black dots), the number of

312 local extrema and their magnitudes (denoted as M_n in **Fig. 7a**, defined as oxygen difference

313 between two adjacent oxygen measurements) are calculated. Then, the normalized frequency

314 histograms of oxygen profiles for different combinations of the number of oxygen extrema and of

315 the extremum magnitude are calculated for three instrumentation types separately (**Fig. 7b-d**). The

316 larger the extremum magnitude, the less frequent the corresponding profiles. Physically, an oxygen

317 profile at a location is not likely to exhibit too large and too frequent oscillations of oxygen

318 concentrations. Thus, the profiles with many/big extrema are likely erroneous. The histogram for

319 Argo profiles differs from those for OSD and CTD because it is based on profiles already validated

320 by the respective DACs. The Multiple extrema check thresholds (black lines in **Fig. 7b-d**) are

321 defined using the histograms as the guidance. The lines crudely correspond to the normalized

322 frequency of 0.01 for OSD and CTD and 0.05 for Argo profiles. The geographical distribution of

323 profiles failing the check is given in **Fig. S6a, d, g**. Argo profiles failing the check can be linked to

324 distinct floats (**Fig. S6g**). The OSD profiles exhibit a higher outlier percentage for the years 1990-

325 2002. The highest rejection rate for the CTD profiles is typical for the years before 2000 (**Fig. S6b,**

326 **e**).
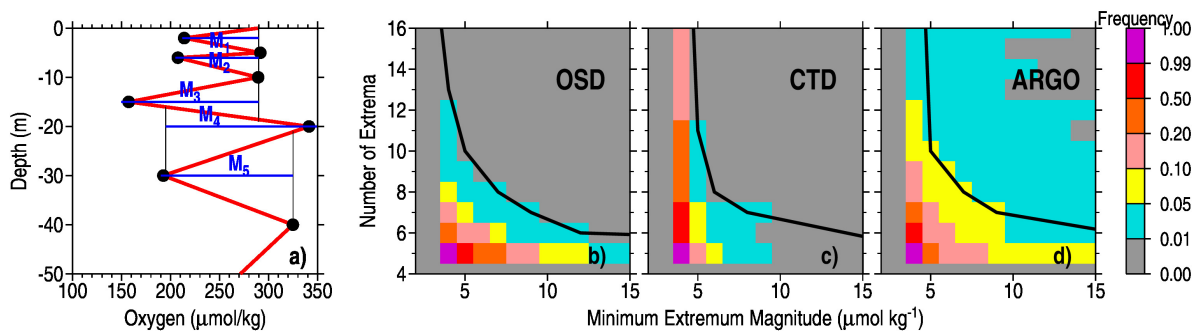
Figure 7. (a) Schematics for the multiple extrema check. Black dots represent the observed values, and the local extrema is defined by M, whereas extremum magnitudes are shown with blue lines. (b-d) Normalized frequency histograms for multiple extrema checks for OSD (b), CTD (c), and Argo (d). The area to the right of the black line corresponds to oxygen profiles failing the multiple extrema check.

327

328 **3.6 Spike check**

329   Spikes are the values at levels that strongly deviate from the values at the nearest levels above

330 and below. For each observed level k, the test value $s = s_1 - s_2$ is calculated, where $s_1 = |p_k - 0.5\ (p_{k-1}-$

331   p_{k+1})|, $s_2=|0.5 (p_{k+1} - p_{k-1})|$ and p denotes the oxygen value. The observation is identified as outliers

332   when the test value s exceeds a threshold value. Due to the larger oxygen variability in the upper

333   layers, we set depth-dependent spike thresholds, which are defined for nine depth layers using

334   accumulated histograms for the test value s (**Fig. 8a**, b for 0-100m, 400-600m as examples). The

335   threshold profile is defined by the 95% frequency at each layer (**Fig. 8c**). The value is chosen

336   empirically but can be tuned when additional QC-ed benchmark datasets become available.

337   Examples of profiles which failed this check are shown in **Fig. 7S**. Data from all instrument types

338   are characterized by a rather homogeneous temporal and spatial distribution of outliers.

339
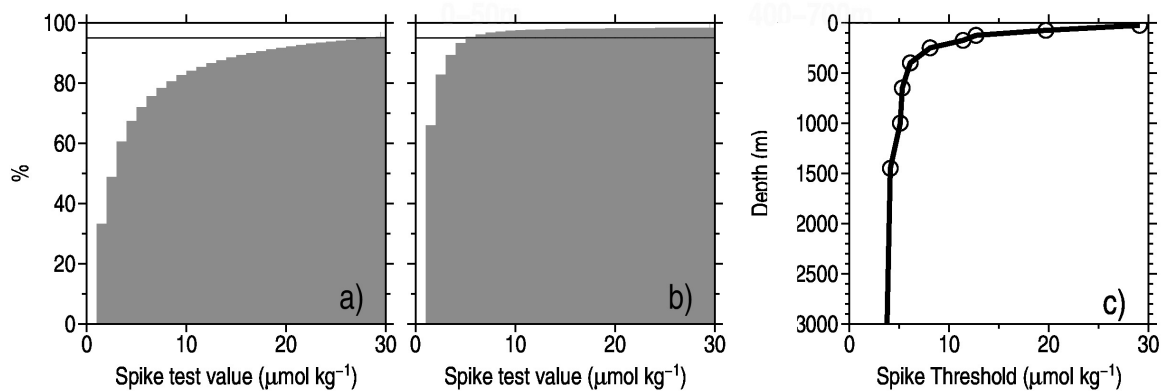
Figure 8. Spike check value histograms (see text for details) for the layer 0-100m (a) and 400-600m (b); spike check value threshold versus depth (c).

340   **3.7   Local climatological oxygen range check**

341   Local climatological oxygen range check is one of the most effective QC modules for

342   identifying outliers compared to other checks because the minimum/maximum thresholds are

343   constrained by the local water mass characteristics. For each 1°×1° latitude/longitude grid point, we

344   calculate min/max thresholds, accounting for the skewness of the data. For calculating

345   climatological ranges, we take the ergodic hypothesis in which the average over time is considered

346   to be equal to the average over the data ensemble within a certain spatial influence radius. Taking

347   into account the skewness of statistical distribution when defining climatological ranges for

348   oceanographic parameters was first suggested by Gouretski (2018), who applied Tukey's box plot

349   method modified for the case of skewed distributions (Hubert and Vandervieren, 2008; Adil and

350   Irshad, 2015). In this method lower (Lf) and upper (Lu) fences are calculated according to formula

351   (1):

352

353     $$[Lf \; Uf] = [\; Q1 - 1.5*IQR*\exp(-SK*|MC|) \quad Q3 + 1.5*IQR*\exp(SK*|MC|) \;], \quad (1)$$

354

355   where Q1, Q3 are quartiles, Q2 is sample median, SK is skewness. MC denotes medcouple, which

356   is defined as MC = median $h(x_i,x_j)$, where $x_i << Q2 << x_j;$ and the kernel function $h(x_i,x_j) = [(x_j-Q2)-$

357     $(Q2-x_i)]/(x_j-x_i)$ (Hubert and Vandervieren, 2008).

358   The local oxygen ranges are constructed using both the OSD and Argo oxygen profiles. The

359   OSD data used to derive the local threshold have undergone the preliminary QC (checks for global

360   oxygen range, spikes, stuck value, multiple extrema), aiming to remove crude outliers to reduce

361   their impact on the local thresholds. This approach is similar to the two-stage thresholding

362   suggested by Yang et al. (2019). The Argo oxygen profiles underwent quality control at the

363   respective DAC centers.

364   The local minimum and maximum thresholds were calculated at 1°×1° grids at a set of 65 depth

365   levels corresponding to the levels implemented for the World Ocean Circulation Experiment/Argo

366   Global Hydrographic Climatology (Gouretski, 2018) using formula (1). Examples of the threshold

367   spatial distribution are presented for two depth levels: 98 meters (level typically located below the

368   seasonal thermocline, **Fig. 9a-c**) and 1050 m (level typically located below the main thermocline,

369   **Fig.9 d-f**). The most striking features are the areas with low minimum oxygen values (oxygen

370   minimum zones, **Fig. 9 a, b**) in the East Pacific, Arabian Sea, Bay of Bengal, Black Sea, and Baltic

371   Sea. The oxygen range map for level 98 m (**Fig. 9c**) shows that the areas with the widest local

372   ranges coincide with minimum oxygen zones. The local range map for the 98 m level also depicts

373   wider ranges in several highly dynamic regions of the Gulf Stream, Malvinas current, and the area

374   north of the Antarctic coast (**Fig. 9c**). During the QC, gridded minimum and maximum local oxygen

375   values are interpolated to the observed levels at profile locations. The geographical distribution of

376   profiles failing the check is given in **Fig. S8a, d, g**, indicating a rather uniform temporal and spatial

377   distribution. A decrease with time of the outlier percentage for OSD data is clearly seen. For CTD

378   data the outlier percentage is high for all levels and years except for the years after 2020. Argo

379   profiles failing the check in many cases can be linked to the data from particular floats (**Fig. S8g**).

380

381   **3.8   Local climatological oxygen gradient range check**

382   The oxygen vertical gradient check aims to identify pairs of levels for which the vertical

383   oxygen gradient exceeds a certain threshold. Threshold values for the vertical gradient (**Fig. 9 g-l**)

384   are calculated using formula (1), similar to the local oxygen ranges. Due to the nonlinearity of

385   oxygen profiles, vertical gradient values depend on the profile's vertical resolution, e.g., from the

386 gap between two neighbors' observed levels. Respectively, oxygen thresholds have been calculated
387 for several depth gaps between 10m and 100m, as Tan et al. (2023) did for the QC of temperature
388 profiles.
389   For level 98 m, the spatial distribution of the oxygen gradient range (**Fig. 9i**) is similar to the
390 spatial pattern of the oxygen range (**Fig. 9c**), with the largest ranges located in the oxygen minimum
391 zones, reflecting the highest oxygen variability in these areas. The region below the main
392 thermocline (**Fig. 9j-l**) is characterized by a much smaller range compared to the 98m level (**Fig.
393 9g-i**). The geographical distribution of profiles failing the check is given in **Fig. S9a, d, g**,
394 indicating a rather uniform temporal and spatial distribution broadly corresponding to the sampling
395 density. For CTD data the lowest outlier percentage is observed after 2000 (**Fig. S9e**).
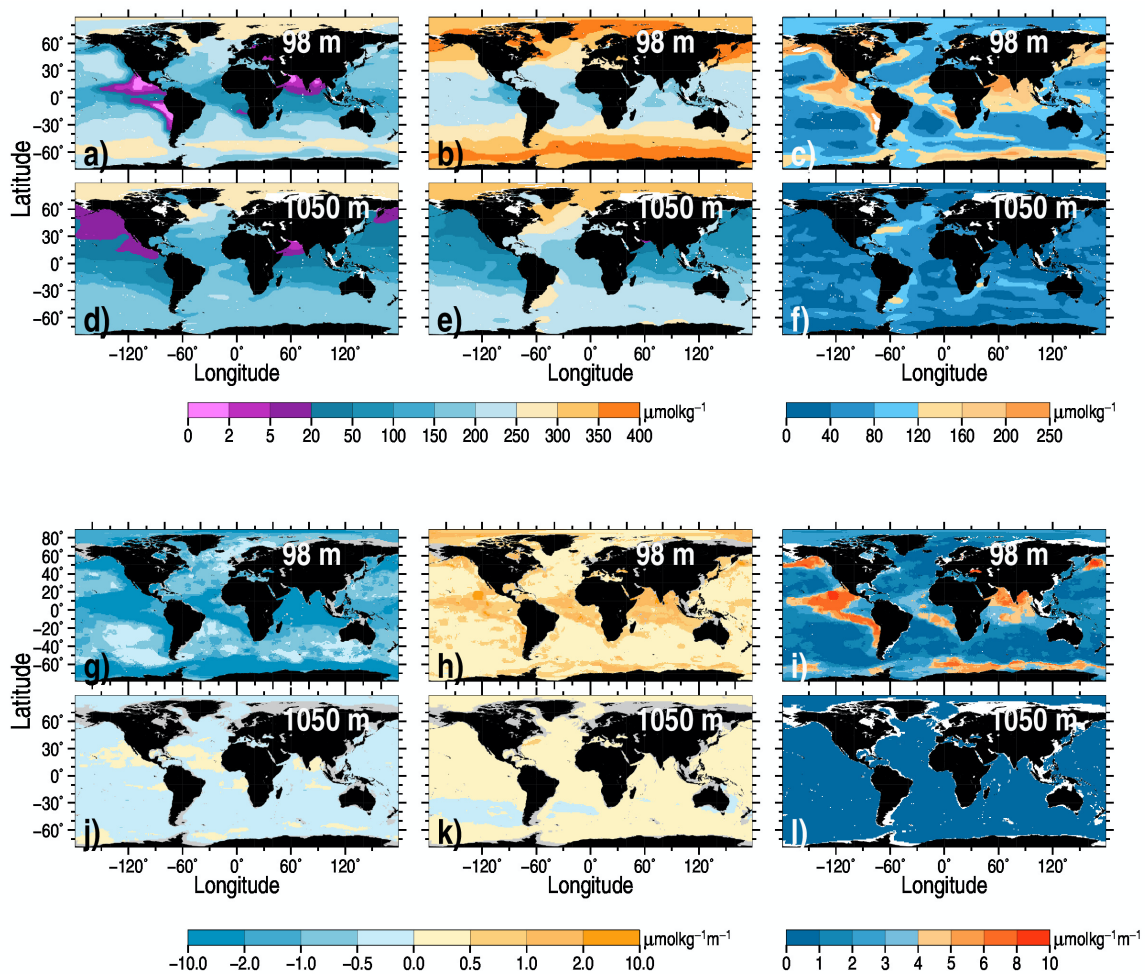
Figure 9. Upper six panels: maps of the lower (a), the upper (b) climatological oxygen threshold, and of the oxygen range (c) for the 98m depth level; d-f) same but for the 1050 m depth level. Lower six panels: maps of the lower (g), the upper (h) the climatological oxygen

vertical gradient threshold, and of the oxygen vertical gradient range (i) for 98 m depth level; j-l) same but for the 1050 m depth level.

396   3.9   Excessive flagged level percentage check

397   After applying all previous quality checks, the percentage of flagged levels for each oxygen
398   profile is calculated to produce histograms in **Fig. 10**. A threshold is set based on these histograms
399   to decide on the quality of the entire profile: we set 20%, 15%, and 30% thresholds for OSD, Argo,
400   and CTD profiles, respectively. If the threshold is exceeded, the entire profile is flagged, and it is
401   suggested that it not be used in future analyses. Both the OSD and Argo datasets are characterized
402   by a low number of profiles with a high percentage of flagged data. In contrast, for the CTD group
403   the histogram (**Fig. 10c**) exhibits a thick and long tail with a significant fraction of profiles having a
404   high percentage of flagged levels.

405   The geographical distribution of profiles failing the check is given in **Fig. S10a, d, g**, indicating
406   a rather uniform temporal and spatial pattern. A decrease of the outlier percentage with time for
407   OSD data is seen after about 2005 (**Fig. S10b**). For CTD data the outlier percentage is high for all
408   years except 2021. Argo profiles failing the check in many cases can be linked to distinct floats
409   (**Fig. S10g**).
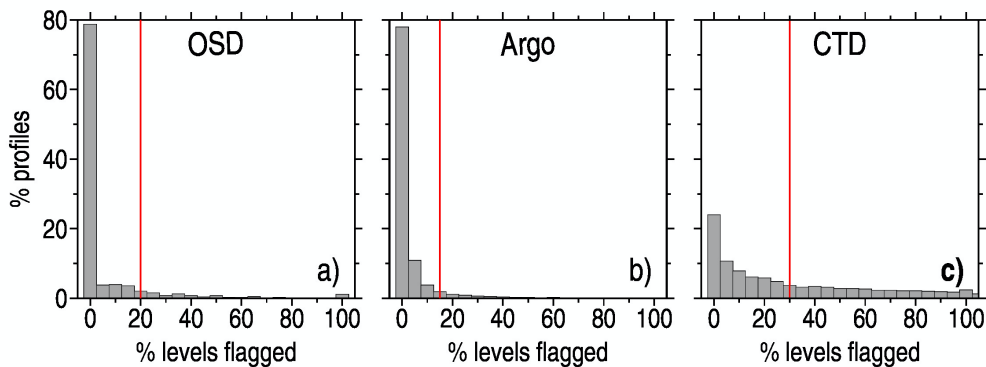
Figure 10. Percentage of oxygen profiles versus percentage of rejected levels per profile for OSD (a), Argo (b), and CTD (c) instrument types.

410   4 Evaluation of the QC procedure

411   Table 2 and **Figure 11** summarize the rejection rates for all ten quality checks for the three
412   instrumentation types separately. The Argo oxygen profiles have the lowest overall rejection rate of

4.8%, with Winkler data quality ranking second best (12.0% outliers). The difference might likely originate from 1) Winkler profiles covering a century-long period of observations, with a poor data quality in the earlier decades; 2) the analyzed Argo oxygen data are represented by adjusted profiles, which have been already quality-controlled.
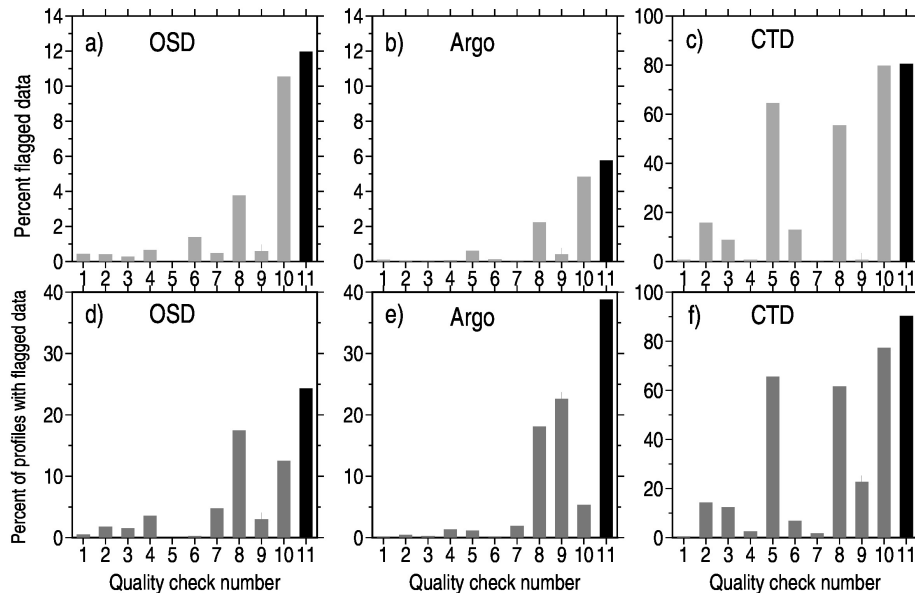
Figure 11. (a-c) Percent of measurements flagged by distinct quality checks for three instrumentation types; (d-f) percent of profiles with at least one measurement flagged. For the description of checks see Table 2. The black bar at the number 11 corresponds to the total percent of flagged data (a-c) and to the percent of profiles flagged by at least one quality check (d-f).

The CTD oxygen profiles have the highest percentage of outliers (overall rejection rate of 80.0% for observational measurements). The significant part of CTD oxygen outliers is attributed to the stuck value check, which searches for profiles with identical or very similar oxygen values at all observed (reported) levels (**Fig, 11a**, check-5). Most of these profiles also fail the local climatological range check. We note that these profiles have also been identified as outliers during the compilation of the WOA18 (Garcia et al., 2018) and WOA23 (Garcia et al., 2023) atlases of dissolved oxygen and have not impacted climatological oxygen distributions presented in these atlases.

As introduced above, the local climatological range check (Check-8 in Table 2) represents the most important quality check and results in the highest percentage of flagged observations and

429 profiles. For OSD, about 17.5% of profiles have at least one measurement flagged by this check.

430 For Argo and CTD profiles, these values are 18.1% and 61.5%, respectively.

431   **Figure 12** shows the percentage of flagged measurement versus time and depth and within one-

432 degree latitude/longitude boxes for three main instrumentation types. The OSD group exhibits a

433 graduate decrease of outlier percentages with time at all depths (**Fig. 12a**), indicating the gradual

434 improvement of data quality with time, especially after the early 1990s, which coincides with the

435 beginning of the extensive observational activities during the World Ocean Circulation Experiment

436 (WOCE). The global spatial pattern of outliers (**Fig. 12b**) is characterized by outlier percentages

437 lower than 5% in most 1° grid cells, with only a few areas exhibiting higher percentages, which can

438 be linked to some particular cruises or observational programs.

439   Oxygen data from Argo floats (**Fig. 12c, d**) are characterized by a low percentage of outliers

440 reflecting the impact of the QC and data adjustments already conducted at DAC centers. We also

441 find no clear time trend in outlier scores. There is an indication of higher outlier percentages in the

442 layer below 1500 m before 2020 (**Fig. 12c**). Strong spatial contrasts in the percentage of Argo

443 outliers (**Fig. 12d**) in most cases can be linked to particular Argo floats.

444   Unlike the OSD Winkler data, CTD oxygen profiles do not suggest a time trend in data quality

445 (**Fig. 12e**). Compared to both OSD and Argo, ship-based CTD oxygen profiles are characterized by

446 a much higher outlier percentage. This is explained through a significant fraction of CTD profiles

447 failing the stuck value check, local climatological range check, and excessive flagged level

448 percentage check (Table 2). The CTD outlier profiles are evenly distributed over the oceans (**Fig.**

449 **12f**). **Figure 12g, h** shows outlier distributions for the profiles which passed both the stuck value

450 and the multiple extrema checks. In this case, most cruise lines (**Fig. 12h**) are characterized by a

451 low outlier percentage, with data quality issues related to a smaller subset of cruises. Finally, we

452 find that the CTD data since 2018 (**Fig. 12g**) exhibit very low outlier scores comparable to those of

453 OSD and Argo float profiles.
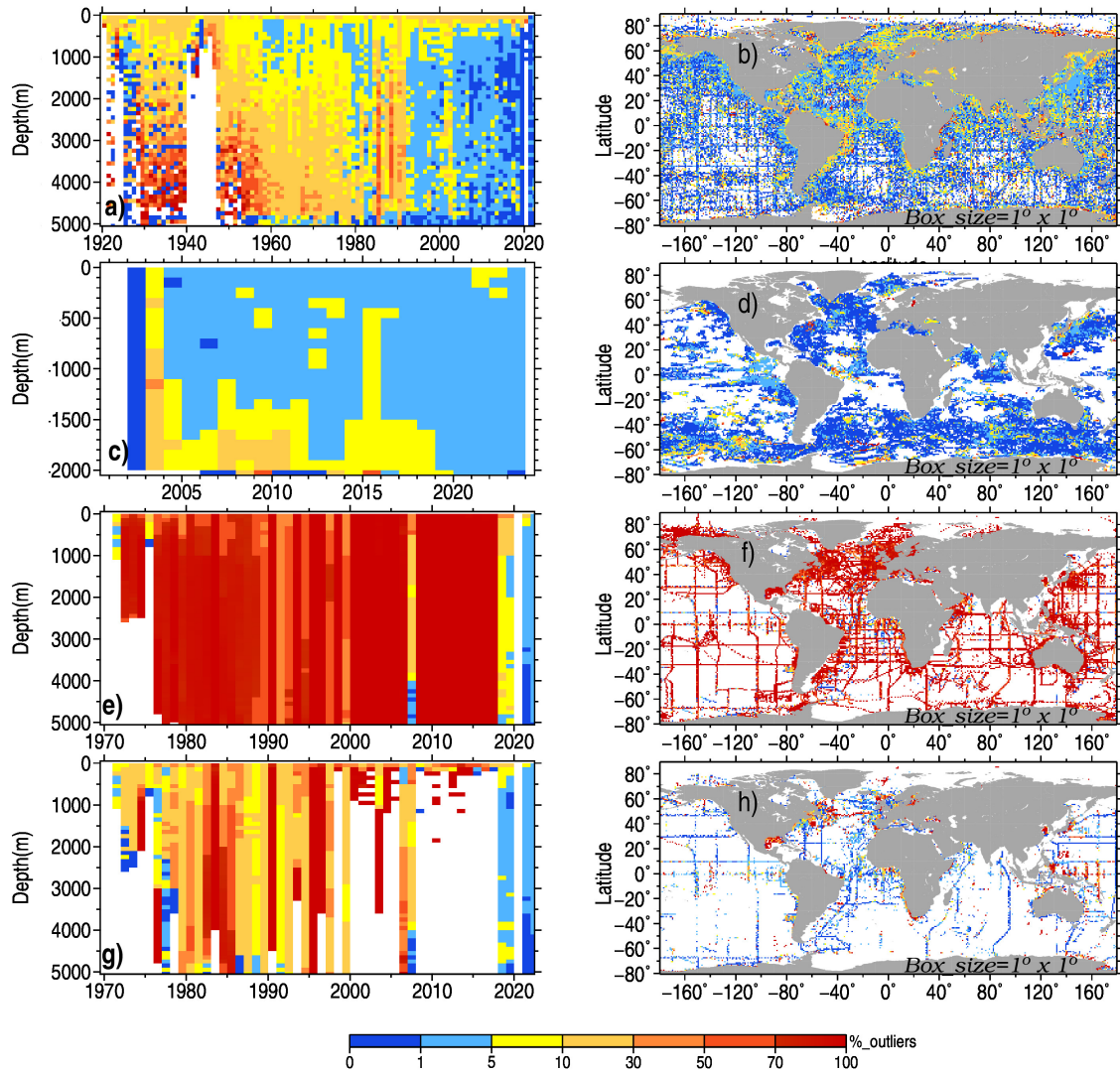
**Figure 12. Percentage of flagged observations in year/depth bins (a) and in 1°
latitude/longitude boxes (b) for OSD oxygen profiles; (c) and (d) same but for Argo oxygen
profiles; (e) and (f) same but for CTD oxygen profiles; (g) and (h) same but for CTD oxygen
profiles which passed multiple extrema and stuck value quality checks.**

454 **Table 2. Outlier score statistics for different instrumentation types**

		OSD		**CTD**		**ARGO**	
No.	Quality Check	% flagged observations	% flagged profiles	% flagged observations.	% flagged profiles	% flagged observations	% flagged profiles
1	Location check	0.422	0.478	0.710	0.521	0.086	0.077

2	Global Oxygen Range at depth levels	0.411	1.751	15.797	14.230	0.041	0.421
3	Global Oxygen Range on T surfaces	0.270	1.492	8.824	12.379	0.009	0.227
4	Maximum oxygen solubility check	0.654	3.548	0.638	2.684	0.081	1.325
5	Stuck value check	0.000	00.000	64.547	65.504	0.043	0.073
6	Multiple extrema check	1.376	0.233	12.846	6.802	0.126	0.057
7	Spike check	0.472	4.732	0.039	1.668	0.012	1.904
8	Local climatological oxygen range check	3.766	17.453	55.398	61.513	2.232	18.118
9	Local climatological oxygen vertical gradient range check	0.584	2.962	0.103	6.207	0.181	13.743
10	Excessive flagged level percentage check	10.538	12.489	79.681	76.853	4.434	4.661
	ALL QC CHECKS	11.968	24.564	80.207	84.392	5.191	29.495

455

5   Benchmarking of the QC procedure using manually controlled datasets

Evaluation of the QC system is a crucial part of the dataset generation. Good et al. (2022) conducted a comprehensive benchmarking exercise to evaluate the performance of automated QC checks for temperature profiles implemented by different research groups, aiming to recommend an optimal set of quality checks. They used several reference datasets with known quality (e.g., bench-marking datasets whose quality was manually evaluated by experts).

Unfortunately, in a deviation from temperature profiles, no community-agreed oxygen datasets exist which could be used for benchmarking. In this study, besides the examples of the QC procedure performance provided for each quality check (Section 3 and Supplementary Material), we use for the bench-marking a comprehensive set of bottle profile data obtained during the World

466 Ocean Circulation Experiment (WOCE) – the largest international oceanographic experiment ever

467 conducted (Wunsch, 2005). To achieve high data quality and consistency between the cruises over

468 the entire period of observations, the WOCE Hydrographic Program Office (WHPO) issued

469 operation manuals (WHPO, 1991), where measurement methods and procedures are described. As

470 shown by Gouretski and Jancke, (2000), the WHPO quality requirements have been fulfilled with

471 the WOCE hydrographic dataset representing a unique global scale high-quality collection of the

472 whole suite of oceanographic parameters. Specifically, the mean inter-cruise oxygen offset was

473 found to be 2.39 µmol kg^{-1}. Upon completing the WOCE, the GO-SHIP program was established in

474 2007 to revise the WOCE hydrographic program by repeating several WOCE lines (Hood et al,

475 2010).

476   Applying our QC procedure to the entire WOCE dataset confirms the high quality of this

477 unique dataset, with only 2.8% of oxygen outliers (**Fig. 13a, b**) from the total of 354028 oxygen

478 measurements for the entire time period 1990-1998. Similar to the entire OSD dataset, the QC

479 diagnostics reflect the progressive improvement of the oxygen data quality over the period of

480 WOCE (**Fig. 13a**). The spatial distribution of outliers for the entire time period (**Fig. 13c**) indicates

481 that the majority of WOCE oxygen profiles have a very low percentage of outliers. For 79% of

482 WOCE oxygen profiles, our QC procedure identified no data outliers. The higher rejection rate is

483 found only for several WOCE lines in the tropical South Atlantic, North-Western Indian Ocean, and

484 the Labrador Sea. We note that, in the same areas, there are data from other cruises which exhibit

485 low outlier percentages, so the flagging cannot be attributed to the spatial selectivity of the QC

486 procedure.

487   The WOD database permits data selection for a large number of observational programs using

488 the respective project identification code. The outlier rejection percentage for the data from 128

489 projects that reported oxygen data is shown in **Fig. 14.** The mean rejection rate over all projects is

490 7%. Apart from WOCE, several outstanding observational programs like GEOSECS (Geochemical

491 Ocean Sections Study) (Craig, 1974), SAVE (South Atlantic Ventilation Experiment) (Larque et al.,

492 1997), CARINA (Carbon dioxide in the Atlantic Ocean) (Falck and Olsen, 2010), and CLIVAR

493 (Climate and Ocean: Variability, Predictability and Change) (Sarachick, 1995) delivered a

494 significant number of high-quality hydrographic data with quality documented in the literature. We

495 note that the four projects with a median year after 1985 (SAVE, WOCE, CARINA, and CLIVAR)

496 are characterized by rejection rates lower than the mean. The 8% outlier rate for one of the largest

497 international GEOSECS experiments conducted in the 1970s only slightly exceeds the mean outlier

498 percentage over all 128 projects.
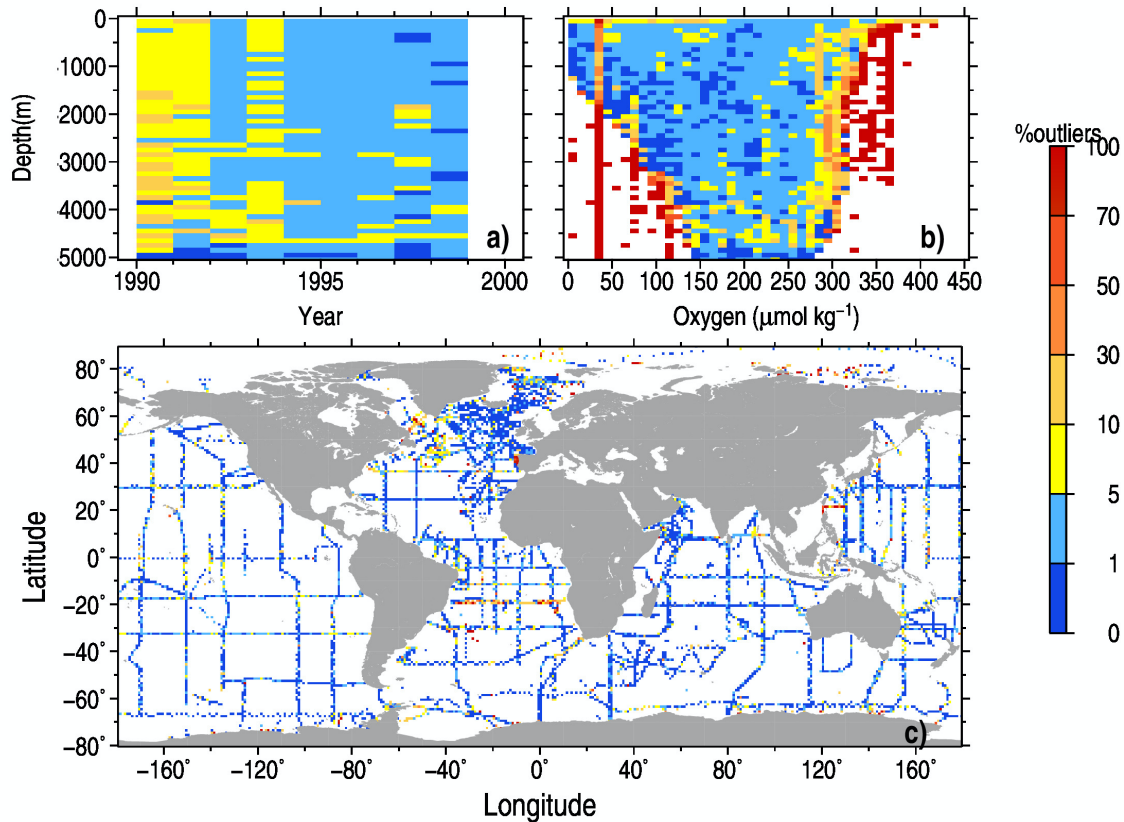
Figure 13. QC statistics for the WOCE dataset: a) percentage of outliers in year/depth bins; b) percentage of outliers in oxygen/depth bins; c) percentage of outliers in 1°×1° squares.

500   Finally, we used the delayed mode quality-controlled Argo data to evaluate the performance of

501   our QC procedure. The Argo dataset used for the current study consists of oxygen profiles reported

502   from 1794 floats. The histogram of the percentage of flagged observations for each Argo float (**Fig.**

503   **15a**) shows that for 90% of all floats, the percentage of rejected observations is less than 15%, with

504   84% of floats exhibiting less than 5% of rejected measurements. We conclude that the QC applied

505   in the DAC centers effectively identifies data outliers for the majority of the floats, resulting in a

506   low outlier percentage (see **Fig. 12 c, d**). The location map of profiles from Argo floats with more

507   than 15% of data flagged over the float lifetime (**Fig. 15b**) shows a rather random distribution

508   throughout the world ocean, with almost all DACs contributing with such floats. We interpreted this

509   result as an implicit confirmation of the ability of our QC scheme to identify data with quality

510   issues.
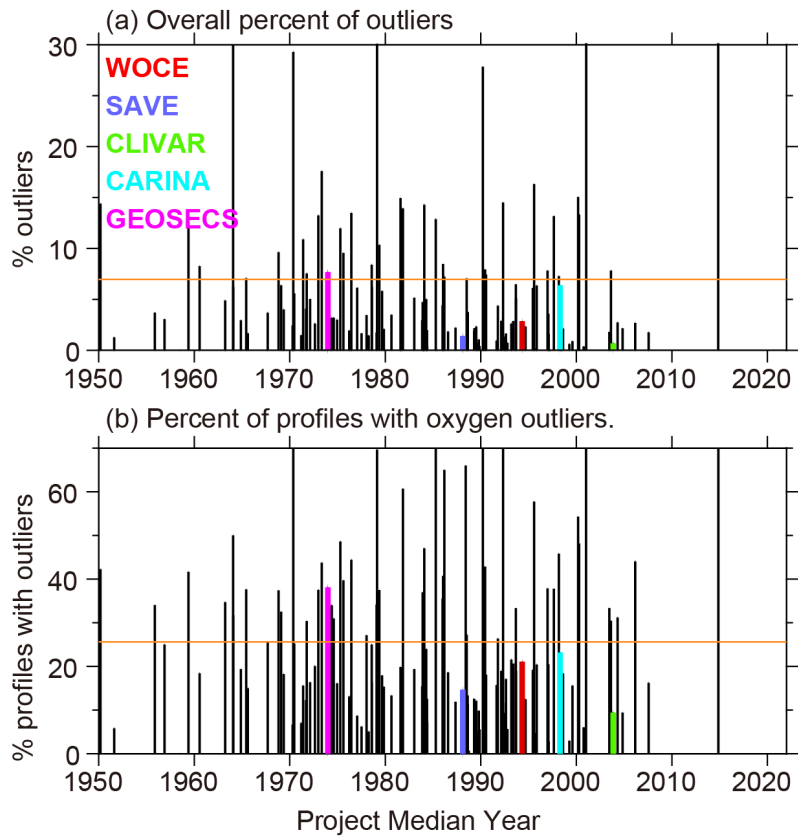
511

Figure 14. Outlier diagnostics for 128 distinct WOD projects (OSD Winkler profiles): a) overall percent of outliers; b) percent of profiles with oxygen outliers. Acronyms and percentages for selected hydrographic projects described in text are shown in color.
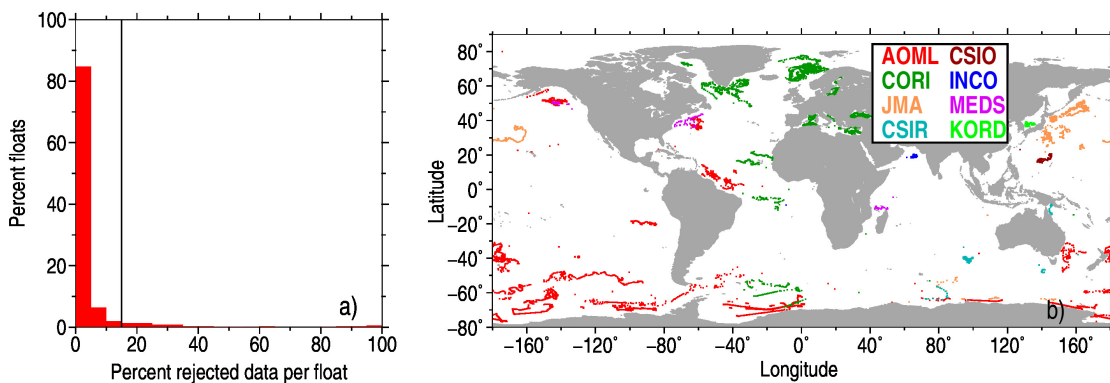
Figure 15. a) percent of Argo oxygen profiles versus percent of flagged data per profile; b) trajectories of Argo floats with more than 15% of flagged data (a total of 127 floats).

6   Bias assessment for sensor oxygen data

The QC procedure described in the previous sections is based on the underlying statistics of the data and aims to identify random outliers. The second step in data QC is estimating the possible systematic errors or biases. These systematic errors may differ depending on the instrumentation type, but the common cause for systematic errors is the absence of the possibility to calibrate the instrument. A classic example provides temperature data obtained by eXpandable BathyThermographs (XBT) where systematic errors are due to the uncertainty in depth, which is calculated from the elapsed time, and the uncertainty in thermistor, which is typically not calibrated (Gouretski and Reseghetti, 2010; Cheng et al., 2014).

In the case of dissolved oxygen, only Winkler oxygen determinations of discrete samples can be considered to be bias-free because the chemical analysis is based on the standard reference, with the replicate measurements having a precision better than 0.4 µmol kg^{-1} (Thaillandier et al., 2018). However, differences in methods and standards between hydrographic cruises suggest a lower level of data precision. Gouretski and Jancke (2000) used the high-quality WOCE one-time hydrographic dataset and conducted a comprehensive analysis of the inter-cruise oxygen differences at the cruise cross-over areas. The analysis was performed in the deep part of the water column (typically below 2000 m), where the time variations of seawater properties are small. For 305 cross-over areas, they estimated the mean difference between WOCE cruises to be 2.40 µmol kg^{-1} with a standard deviation of 2.37 µmol kg^{-1}. Considering stringent criteria for the WOCE hydrographic program, this estimate can be considered to represent an approximate precision of the Winkler method in application to real hydrographic data. As noted by Golterman (1983), the Winkler method still represents the most precise determination of dissolved oxygen. In spite of some modifications over time, the principle of the method is unchanged. In the following, we describe residual biases for CTD and Argo profiles. The term "residual" is used because CTD oxygen profiles are often adjusted on Winkler bottle samples, and Argo oxygen profiles used in our study undergo adjustment procedures at the respective DACs.

The use of electrochemical and optical oxygen sensors in oceanographic practice has two main aspects. First, these sensors permitted a significantly higher rate of data acquisition and a much finer vertical resolution than bottle data. Secondly, they made the observational process much easier than bottle samples, which need chemical titration in the laboratory. However, like other electronic sensors, oxygen sensors are prone to offsets and drift. Takeshita et al (2013) analyzed data from 130 Argo floats and found a mean bias of -5.0 % O_2 saturation at 100 % O_2 saturation. Bittig et al.

544 (2018) explained this negative bias by the reduction of O_2 sensitivity proportional to oxygen

545 content, with the decrease of sensitivity being on the order of several percent per year. Optode drift

546 characteristics require regular calibration. Use of reference Winkler profiles is possible only for the

547 ship-based CTD oxygen sensors (mostly electrochemical sensors) if CTD rosette water samples are

548 obtained simultaneously with sensor profiles and are analyzed for oxygen during a cruise (Uchida et

549 al., 2010). For unmanned autonomous platforms like Argo, the direct comparison with reference

550 Winkler data is limited to samples from the hydrographic casts conducted during the float

551 deployment. Bittig et al. (2018) recommended adjusting optode data on oxygen partial pressure

552 primarily by the gain (Argo Quality Control Manual, 2021). If no previous delayed-mode

553 adjustment is available, the basic real-time adjustments are performed based on the oxygen

554 saturation maps provided by the WOA digital climatological atlas (Thierry et al., 2021). In case a

555 delayed-mode adjustment is not available after one year, the re-assessment of the gain factor is

556 recommended. Uncertainty in underlying optode calibration and time drift characteristics leads to

557 errors in adjusted data.

558

559 **6.1   Bias assessment method**

560   We aim to assess the magnitude of the possible overall residual bias for CTD profiles and

561 adjusted Argo profiles by comparing these profiles with collocated reference discrete samples. The

562 data from 10 national DACs were used for this analysis, for which both unadjusted and adjusted

563 oxygen profiles are available. Data centers and the respective number of oxygen profiles are given

564 in Table 1. Data using the Winkler method are used as reference data for the comparison with

565 collocated Argo oxygen profiles.

566   For the current analysis, we selected a 100 km threshold distance within which two profiles are

567 spatially collocated. To decide upon the choice of the optimal maximum time difference between

568 Argo and reference profiles, we calculated median oxygen offsets increasing threshold value for the

569 time separation between a pair of profiles (**Fig. 16a**). Increasing the temporal collocation bubble

570 leads to the increase of the bias magnitude in agreement with the assumption that the older

571 reference data are richer in oxygen compared to the more recent data. Below 1000 m depth, the

572 difference between the median offsets for the temporal collocation bubble of 5 and 50 years is about

573 3.5 µmol kg^{-1}, corresponding to a deoxygenation trend of about 0.7 µmol kg^{-1} per decade. This

574 estimate can be compared with 0.75 µmol kg^{-1} per decade reported by Gregoire et al. (2021). As

575 **Fig. 16c** suggests, the overall offset estimate below 1000 m stabilizes after the time difference

576 threshold of 5 years. The extension of the temporal bubble for more than 7 years leads to the

577 progressive increase of the bias magnitude, which we attribute to the impact of the general

578 deoxygenation. Based on these calculations, the 5-year threshold was selected as the maximum time

579 separation between collocated profiles. For this threshold value, the number of collocated pairs

580 below 1000m depth is about 10000 (**Fig. 16b**). A step-wise decrease of the number of collocated

581 pairs below 950 m is explained by a significant part of reference profiles being limited to the upper

582 1000-meter layer. These calculations suggest that about 1000 collocated pairs are required for stable

583 offset estimates.
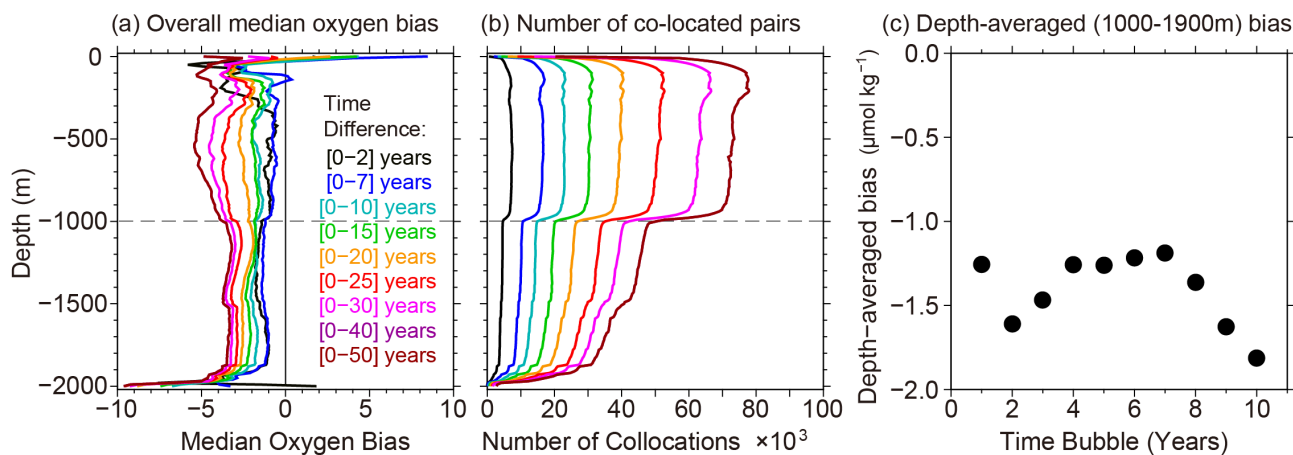
584

Figure 16. a) Overall median oxygen bias versus the size of the temporal collocation bubble; b) number of collocated pairs for different choices of collocation bubbles; c) depth-averaged (1000-1900m) bias versus time bubble size.

585

586   The number of Argo profiles having collocations with discrete ship-based Winkler profiles is

587 shown in Table 1. No collocated Winkler profiles are found for the Argo profiles from the two

588 Korean DACs. Profiles from these DACs are restricted within a relatively small area east of the

589 Korean peninsula. The four largest contributors of Argo data (AOML, Coriolis, JMA, and CSIRO)

590 comprise up to 90% of all Argo profiles having collocations with reference profiles.

591

592 **6.2   Overall bias characteristics of unadjusted and adjusted Argo oxygen data from DACS**

593   The normalized frequency histograms (**Fig. 17**) characterize the spread of individual bias

594 estimates around the distribution mode. These histograms are based on all Argo profiles having

595 collocations with reference Winkler data. In these histograms, for each depth bin, the number of

596 values in each bias bin is normalized by the number for the most populated bias bin at each depth

597 level to account for the decrease of data with depth. The histograms are shown for raw (unadjusted)

598 (**Fig. 17a**) and adjusted Argo profiles (**Fig. 17b**). The adjustment procedures applied at different

599 DACs reduce the spread of the individual bias estimates and the skewness of the bias distribution,
600 with the overall median bias of 10-12 µmol kg⁻¹ for unadjusted data and 1-2 µmol kg⁻¹ for adjusted
601 data. As suggested by the bias distribution with depth, we estimate residual bias using the collocated
602 data below 1000 m depth, where the bias spread reduces significantly compared to the upper part of
603 the water column.

604
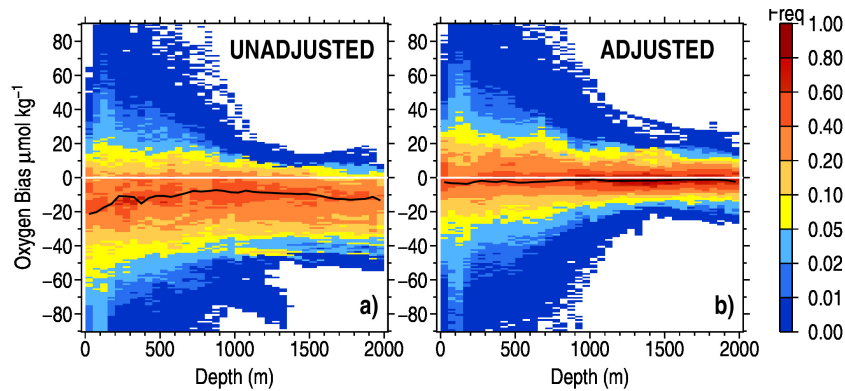
Figure 17. Normalized histograms of the unadjusted (a) and adjusted (b) Argo oxygen bias versus collocated Winkler profiles. The black lines show the median bias value.

605

606 **6.3 Residual Oxygen Biases for distinct oxygen sensor**

607 A total of 11 oxygen sensor models were implemented on Argo BGC floats, with 8 sensor
608 models found among Argo profiles having collocations with reference data (see Table 3). **Figure 18**
609 shows the yearly number of Argo profiles that have collocations with reference data and are
610 equipped with different models of oxygen sensors. The SBE43 series sensors are electrochemical
611 Clark-type sensors, whereas all other models are optical sensors (optodes). Since the beginning of
612 the 2000s, several models of optodes have been implemented in BGC Argo floats. The two most
613 widespread sensors are AANDERAA 3830, implemented between 2004 and 2018, and the newer
614 model AANDERAA 4330 used since 2010. The majority of Argo floats from the three largest
615 AOML, Coriolis, and JMA datasets have been equipped with this sensor. Data from AOML,
616 Coriolis, JMA, and CSIRO include oxygen profiles obtained by means of several sensor models.
617 The other four DAC subsets of data are represented by a single sensor model:
618 AANDERAA_OPTODE_4330 prevails in the data from INCOIS, CSIO, and BODC, and

619   AANDERAA_OPTODE_3830 is typical for MEDS data. AROD_FT and ARO_FT optodes have

620   been implemented only on Argo floats managed by JMA.

621

622   **Table 3. Oxygen sensors installed on BGC Argo floats**

N	Oxygen Sensor Model	Number of Argo profiles	Number of Argo profiles collocated with Winkler profiles
Optode sensors			
1	AANDERAA_OPTODE_4330	160261	16112
2	AANDERAA_OPTODE_3830	49049	8234
3	AANDERAA_OPTODE_3835	405	0
4	AANDERAA_OPTODE_4831	454	0
5	SBE63_OPTODE	16775	1978
6	SBE83_OPTODE	462	0
7	ARO_FT	2792	618
8	AROD_FT	370	31
Clarke-type sensors			
9	SBE43F_IDO	12234	2341
10	SBE43I	9620	1046
11	SBE43_IDO	2173	246

623
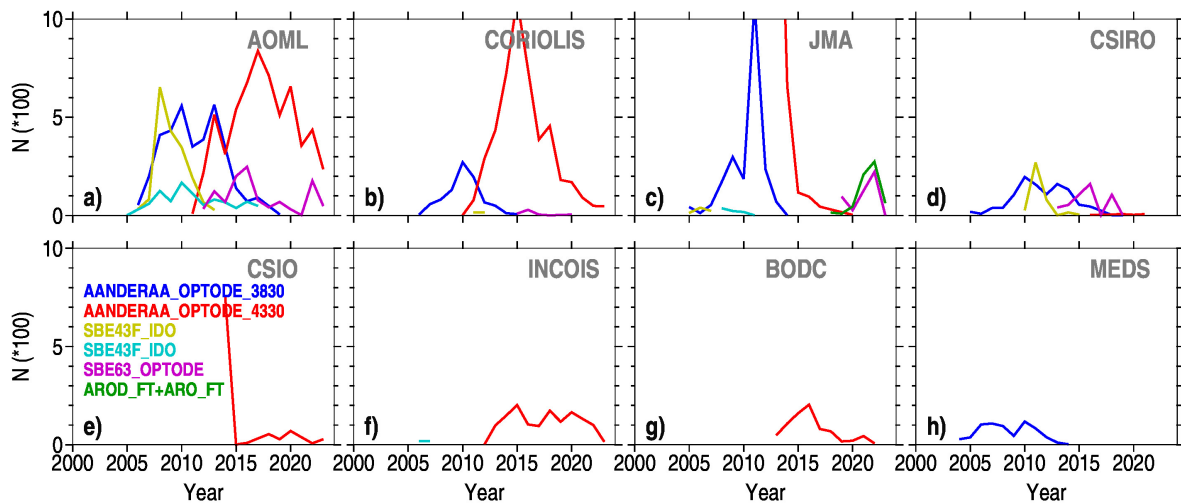
Figure 18. Yearly number of BGC Argo profiles equipped with different types of oxygen sensors (colored lines, see sensor attribution in plate e)). (a) AOML, (b) Coriolis, (c) JMA, and (d) CSIRO, e) CSIO, f) INCOIS, g) BODC, h) MEDS.

According to the Argo Quality Control Manual (Thierry et al., 2021), several adjustment procedures can be applied to unadjusted data (adjustment to climatology, nearby Winkler samples, or in-air data). The adjustment results may depend on many factors, such as the subjective decision of the operator in a DAC, the use of a specific software, the availability of the respective reference data, and other factors. If a climatology is used as a reference, the Argo oxygen values will be adjusted to the median year of a climatology, which can differ by several decades from the year of an Argo profile. In such cases, the long-term deoxygenation trend of the world ocean might impact the results of the adjustment procedure. Differences in the applied adjustment procedures may potentially result in DAC-specific residual offsets. Considering these two main causes for biases in sensor oxygen data, we calculated profiles of overall oxygen biases versus depth (e.g. biases based on the data from all years) for six sensor models (1, 2, 5, 6, 8, and 10, see Table 3) and for six DACs which provided a sufficient number of collocated pairs (**Fig. 19**).

The number of available collocations with reference Winkler profiles varies by two orders of magnitude for different DACs. Since reference bottle data often cover only part of the upper 2000-meter layer, the number of collocated pairs also changes over depth, with the main step-wise decrease seen around 1000 m. However, our calculations suggest that changes in the number of collocated pairs over depth do not significantly impact the diagnosed bias. In order to reduce the effect of the varying geographical sampling pattern over depth, only Argo profiles deeper than 1000

m were used for bias calculations. **Figure 19** shows a much higher variability of diagnosed biases in the upper part of the water column due to a stronger temporal and spatial oxygen variability. However, in the layer below 1000 m (e.g., crudely below the main thermocline), all profiles indicate much smaller variations over depth, and in the following discussion, we will focus on biases within this layer.

For almost all oxygen sensors, the overall bias exhibits a characteristic hook below about 1900-1950 meters. Such hooks on Argo oxygen profiles were found by Thallander et al., (2018). The hook can reflect the adjustment of the oxygen sensor at the beginning of the float ascending. Further we note that Clarke-type sensors from SBE43 series are characterized by a positive oxygen bias below 1000 m, whereas the majority of optoids is characterized by negative biases, with the exception of SBE63 profiles in CSIRO data.

Another feature common to AANDERAA optodes and SBE43-series sensors is the dependence of bias on depth (pressure). For one and the same sensor model, the slope of the bias profile differs among the DACs. The most clear dependence on pressure is seen for the SBE43F IDO and SBE43I models for AOML data (**Fig. 19c, d**) and for AANDERAA_3830_OPTODE for the four largest DAC datasets (**Fig. 19a**). It is known that dissolved oxygen measurements by SBE43-IDO series sensors are influenced by changes of sensor membrane characteristics due to temperature and pressure. Depending on the sensor's time-pressure history, these changes have long time constants, resulting in hysteresis at depths greater than 1000 meters (Thierry et al., 2021). Until now, there has been no effective method for adjusting the pressure effects of these sensors on profiling floats under operation. Data from all optodes also require adjustments for pressure effects (Bittig et al., 2015). Increasing pressure reduces the oxygen concentration inside the sensing membrane (which is relevant for luminescence quenching) by ca. 3.0 - 5.5% per 1000 dbar. The optodes are thus expected to show lower oxygen under pressure, which is confirmed by our **Fig. 19a, b** for all DACs except JMA.

Also shown in **Fig. 19** are estimates of mean biases calculated for the layer 1000-1900m ($B_{1000-1900m}$). The lower boundary of 1900m was selected in order to exclude the depth range where bias profiles exhibit characteristic hooks described above. In order to assess the stability of the overall biases shown in **Fig. 19**, we calculated the time series of the bias for the layer 1000-1900m for six most numerous sensor models (**Fig. 20**). The changes of the diagnosed biases over time indicate a certain degree of sensor stability with biases typically retaining the same sign throughout the entire period of observations. We attribute at least a part of this layer's apparent bias time variability to the changes in the geographical sampling and the differences in the reference data.
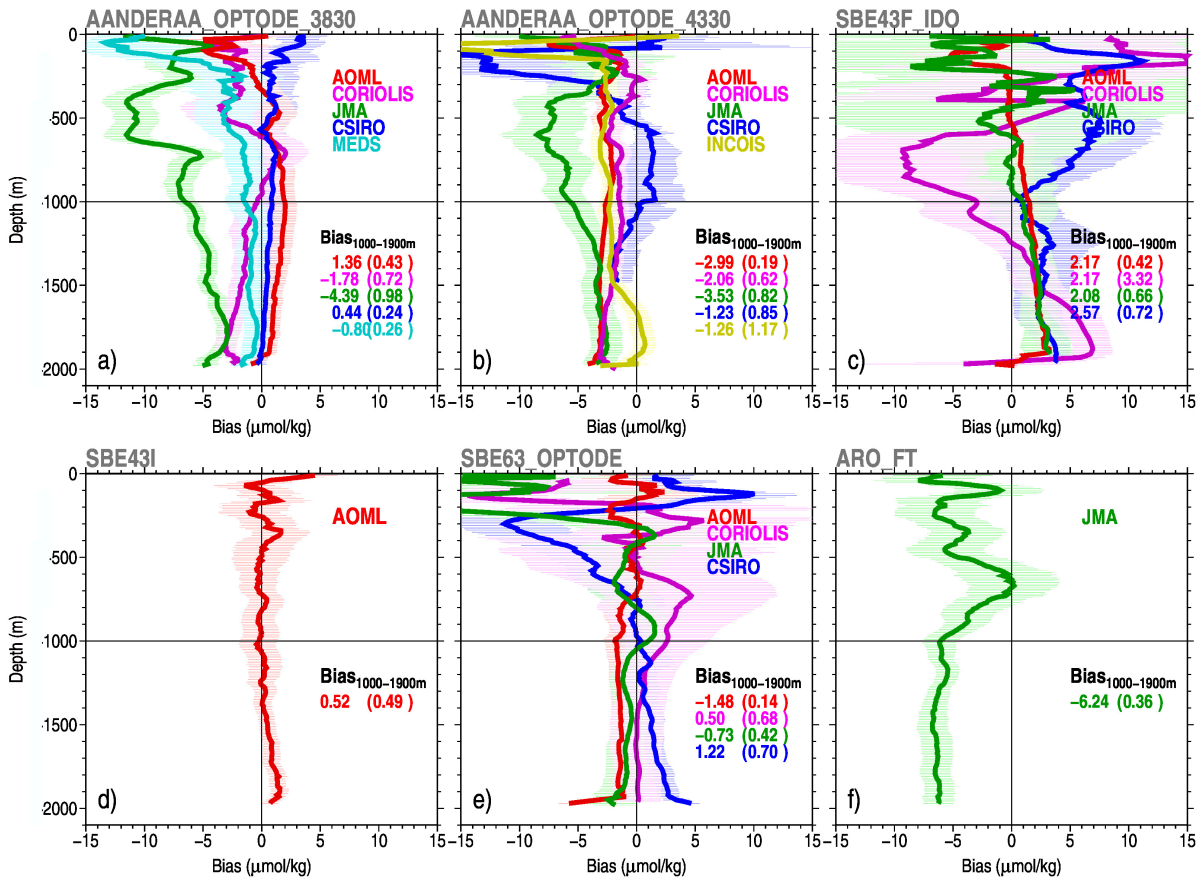
679 **Figure 19. Overall oxygen biases for six oxygen sensor models: a)**
680 **AANDERAA_OPTODE_3830, b) AANDERAA_OPTODE_4330, c) SBE43F_IDO, d) SBE43I,**
681 **e) SBE63_OPTODE, f) ARO_FT. Bias profiles are shown for the six largest DAC datasets**
682 **(colour lines). Values of the average bias for the layer 1000-1900m (B$_{1000\text{-}1900m}$) are shown in**
683 **the lower right part of each panel, with standard errors given in parentheses. Light colour**

Figure 20. Residual oxygen bias for the layer 1000-1900m versus time. Vertical bars show standard error with the number of degrees of freedom equal to the number of distinct floats. Each value corresponds to the bias averaged within the five-year time window. Calculations are shown for the data from distinct DACs: a) AOML, b) Coriolis, c) JMA, d) CSIRO.

In order to assess the stability of the overall bias estimates shown in **Fig. 19**, we calculated time series of the average bias within the layer 1000-1900m for six most abundant sensor models (**Fig. 20**). The changes of the diagnosed biases over time indicate a certain degree of sensor stability with biases typically remaining positive or negative over the entire period of observations. At least part of this apparent time variability may be due to the changes in the number of collocated pairs and their geographical distribution over time. Considering the strong limitation imposed by the number of available collocated pairs, we suggest overall constant bias corrections for different sensors and DACs (Table 4). These corrections correspond to the residual biases in the layer 1000-1900 m (see **Fig. 19**).

Table 4. Sensor-specific bias corrections for data from different DACs[*)]

	Sensor model	AANDERAA_OPTODE_3830	AANDERAA_OPTODE_4330	AROD_FT, ARO_FT	SBE43F_IDO	SBE43I	SBE63_OPTODE
1	AOML	1.36(0.43)	-3.22(0.19)		2.17(0.42)	0.52(0.42)	-1.07(0.16)
2	Coriolis	-1.78(0.72)	-2.06(0.62)		2.17(3.32)		0.50(0.68)
3	JMA	4.38(0.99)	-3.19(0.52)	-6.24(0.36)	2.08(0.67)	0.52	-0.74(0.42)
4	CSIRO	0.44(0.24)	-1.23(0.70)		2.57(0.72)		1.22(0.70)
5	CSIO		-2.43				-0.02
6	INCOIS		-2.43			0.52	
7	BODC		4.00(2.07)				
8	MEDS	-1.09	-2.43				-0.02
9	KORD	1.09			2.25		
10	KMA		-2.43				

[*)] Bias corrections are given in μmol/kg. Values in parentheses show standard errors. If standard error is not shown the correction indicates a guess value equal to the mean of values with standard error estimate. Corrections indicated in the table should be subtracted from the reported oxygen value. Empty boxes correspond to the sensors which are absent for a specific DAC.

Finally, overall biases were calculated for the data from eight distinct DACs (Korean datasets from KORDI and KMA are relatively small and do not have collocations with reference cruises available for this study). Biases were calculated for the original data (QC-ed and adjusted by DACs) and for the data corrected for residual biases according to Table 4 (**Fig. 21**). For all DACs, the suggested bias corrections led to the reduction of the overall bias. AOML, CSIRO, and MEDS data

**Figure 21. Overall mean Argo oxygen offsets versus Winkler profiles for distinct DACs: a)
AOML, b) Coriolis, c) JMA, d) CSIRO, e) INCOIS, f) MEDS, g) CSIO, h) BODC. Offset
profiles for DAC-adjusted data and for the data corrected for residual biases (Table 4) are
shown in red and blue, respectively. Standard error bars (light shading) are calculated using
the number of distinct floats at each level as the number of degrees of freedom. Green lines
show number of collocated pairs in thousands.**

6.4 Residual Oxygen Biases for CTD oxygen sensors

We conducted similar bias calculations for the CTD oxygen profiles obtained by both
electrochemical and optical sensors. Only CTD data which passed all QC checks were used for the
bias estimation. Unlike Argo profiles, the CTD oxygen sensor data can be adjusted on the
simultaneously collected bottles analyzed in the ship laboratory using the Winkler method

(Taillandier et al., 2018). Unfortunately, it is not possible to identify profiles with such adjustments within the WOD archive because of missing metadata. As noted by Boyer et al. (2018) "in many cases, the dissolved oxygen … data are uncalibrated and not of high quality. Information on whether these variables are calibrated is not usually supplied by the data submitter". As noted by Uchida et al. (2010) calibration of oxygen sensor profiles is not straightforward, requires some expertise, and depends on the quality of the reference data. Saout-Grit et al. (2015) described the calibration procedure for SBE-43 sensor done by fitting to reference Winkler data and found a time trend in residuals during the analyzed cruise. WOD archives the data submitted by the data producers and other resources. Thus, the data quality and calibration procedure of the CTD oxygen data are likely inhomogeneous.

For 0-1900 m, we find an overall CTD oxygen offset of about 0.25 µmol kg^{-1} (median) relative to the Winkler data over the 1960-2022 period, which is much smaller than Argo oxygen biases ranging from -3.72 (JMA) to 0.76 µmol kg^{-1} (CSIRO) (see **Fig. 19**). Similar to Argo data the offset distribution above 1000 m level (**Fig. 22e**) exhibits stronger spread than that below 1000 m. The median offset for the layer 1000-2000 m is 0.25 µmol kg^{-1}. Grégoire et al. (2021) indicated that "*the uncertainty associated with the last generation of O$_2$ sensors that uses the best calibration and calculation methods amounts, in the best case at ~2 µmol kg^{-1}*". Therefore, the overall median offset of 0.25 µmol kg^{-1} identified by this study is well within the expected uncertainty of the CTD sensors. Besides, there is no spatial uniform pattern for the CTD offsets (**Fig. 22d**), implying that this offset might not be systematic. Further investigation of the offsets for different cruises (figure not shown) indicates that the offset varies cruise by cruise and year by year. Therefore, in this study, we decided not to adjust the CTD data before the offset can be further confirmed after a cruise-by-cruise investigation, and the underlying reasons for the bias can be understood.

759
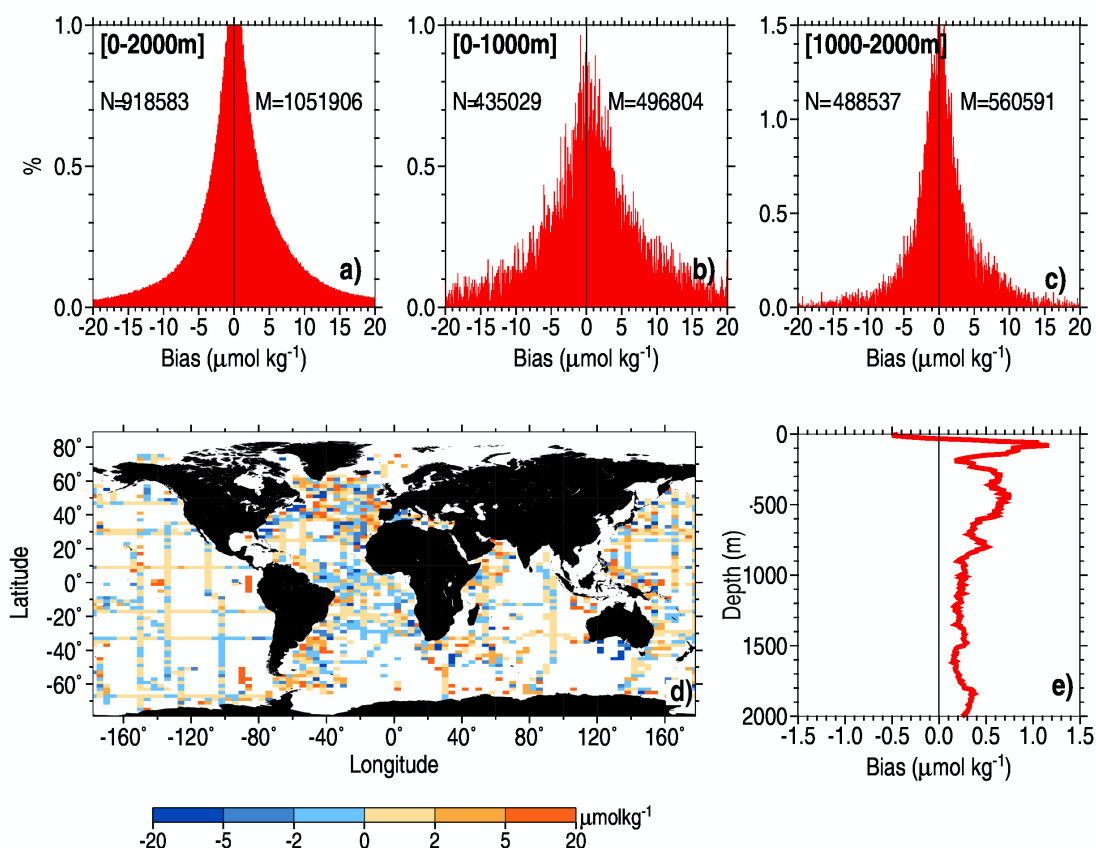
Figure 22. Statistics of the CTD oxygen bias relative to co-located Winkler data. Histograms of layer-averaged bias for 0-2000 m (a), 0-1000 m (b) and 1000-2000 m (c). Number of negative (N) and positive (M) bias values is shown respectively on the left and right side of each histogram. (d) median of depth-averaged bias (1000-2000m) in 2°×4° grid boxes; (e) overall median CTD oxygen offset as a function of depth.

760

7. Impact of quality control and bias adjustment on estimating oxygen changes

Applying the QC and bias adjustment to historical *in situ* oxygen data is expected to impact the derived ocean oxygen changes on various spatial/temporal scales. To illustrate this impact, we implemented the new Auto-QC system for all oxygen data and adjusted the Argo data based on the approach described in Section 6. Based on these data, we applied the mapping method (Ensemble Optimal Interpolation approach with a Dynamic Ensemble from climate model simulations, EnOI-DE) proposed by Cheng et al. (2017, 2020) to spatially interpolate oxygen data, yielding a spatially complete gridded global ocean oxygen dataset. Because of the limited spatial coverage of oxygen data, we combine each successive three years of data to derive oxygen fields for each calendar year.

Respectively, the oxygen time series are based on these fields. The reconstruction is only done for the upper 2000 m because of the insufficient in situ data in the abyssal layers. The resultant oxygen field is denoted as "after QC/adjustment". To show the impact of QC and adjustment on the oxygen changes estimate, we also applied the same method to the data without QC (e.g. with only several crude QC checks applied to remove most likely erroneous values, including overall range checks, solubility check, and spike check) and without Argo adjustments. The resultant field is denoted as "before QC/adjustment".

The long-term mean states (e.g., the climatology, reconstructed using all data between 1990-2022 based on EnOI-DE approach) of the upper 1000 m oxygen before and after QC/adjustment are very similar (**Figs. 23a, b**). One reason is the EnOI-DE method (as any mapping approach) has a smoothing effect, so the erroneous data is less visible behind high spatial variability. This indicates the robust large-scale pattern, where the oceans in the low latitudes have lower oxygen concentrations than in the higher latitudes because of the water temperature and ocean circulation difference. The Eastern Pacific and North Indian Oceans show even lower oxygen levels because of the subsurface oxygen minimum zone. The difference between oxygen climatologies calculated before and after QC/adjustment ranges from -15~15 μmol kg^{-1} but differs at different locations (**Fig. 23c**). The zonal mean difference is smaller (-3~1 μmol kg^{-1}) because of the error cancellation at each latitude (**Fig. 23d**).

The QC/adjustment also impacts the annual cycle (including both phase and magnitude) of the global mean oxygen changes (**Fig. 23e**). Examples for the layers 0 – 100 m (representing the upper seasonal change layer), 100 – 600 m (representing the main thermocline) and 0 – 2000 m (showing the ocean oxygen inventory) are shown in **Fig. 23e**. For 0 – 100 m, the mean oxygen level shifts from negative to positive in November after QC/adjustment but in September before QC/adjustment. The magnitude of the annual cycle, if simply defined as the difference between the maximum and minimum of the 12-month climatology time series, is 1.45 μmol kg^{-1} but slightly reduced after QC/adjustment (1.22 μmol kg^{-1}). The magnitude of the 100 – 600 m and 0 – 2000 m

796   annual cycle has also been reduced after QC/adjustment (1.18, 0.55 µmol kg⁻¹ before

797   QC/adjustment and 0.79, 0.48 µmol kg⁻¹ for 100 – 600 m and 0 – 2000 m, respectively, **Fig. 23e**).
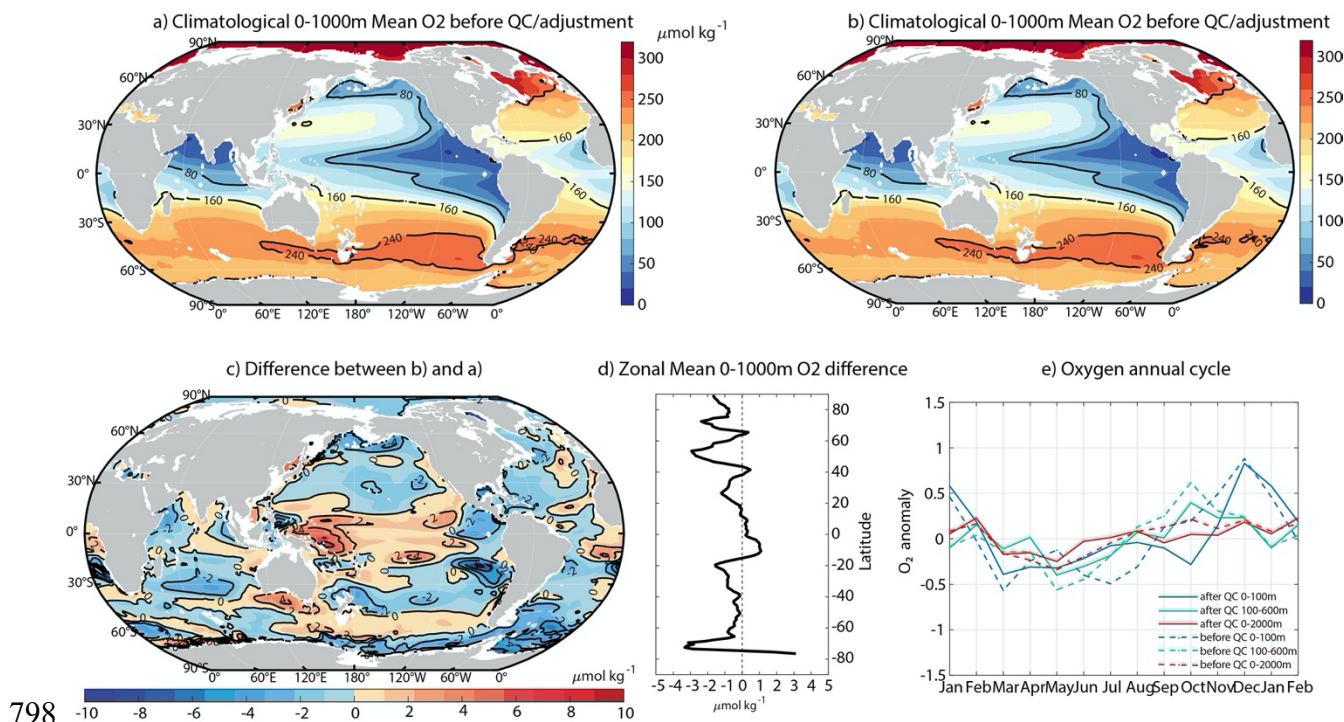
799   **Figure 23. The climatological upper 1000 m oxygen field before (a) and after (b)**

800   **QC/adjustment, with their spatial difference shown in (c) and zonal mean differences in (d).**

801   **The annual cycle (relative to the climatological annual mean level) before (dashed line) and**

802   **after (solid line) QC/adjustment are compared in (e) for different vertical layers. The**

803   **climatology field is reconstructed by combining all data within 1990-2022 with EnOI-DE**

804   **mapping method (Cheng et al. 2017, 2020).**

805

806   The QC and adjustment also impact the estimates of long-term oxygen changes, for example

807   the global deoxygenation estimates for 0 – 100 m, 100 – 600 m and 0 – 2000 m layers depicted in

808   **Fig. 24**. After QC/adjustment, the standard deviation of the time series is decreased from 1.71 (0 –

809   100m), 2.37 (100 – 600m), 1.60 (0 – 2000m) to 1.62 (0 – 100m), 2.24 (100 – 600m), 1.44 (0 –

810   2000m) µmol kg⁻¹, showing a reduced variability in global oxygen time series after QC/adjustment.

811   This indicates a reduction of noise, which is mainly attributed to both QC and Argo adjustment. For

812   example, before QC/adjustment, there was a big global 0-100m deoxygenation of ~ 3 µmol kg⁻¹

813   from 1995 to 1996, which is likely non-physical and spurious. Such change disappeared after

814   QC/adjustment (**Fig. 24**). The linear rate of deoxygenation differs for the two tests as well: -0.77 ±

815   0.43 (0 – 100m), -1.45 ± 0.30 (100 – 600m), -0.95 ± 0.30 (0 – 2000m) μmol kg^{-1} dec^{-1} before

816   QC/adjustment and -0.90 ± 0.38 (0 – 100m), -1.37 ± 0.40 (100 – 600m), -0.84 ± 0.41 (0 – 2000m)

817   μmol kg^{-1} dec^{-1} after QC/adjustment. The linear trend is calculated by the ordinary least square

818   regression with a 90% confidence interval shown (accounting for the reduction in degree of

819   freedom). The deoxygenation rates are reduced after QC/adjustment for both 100 – 600m and 0 –

820   2000m, mainly because of the Argo adjustment, which shifted the oxygen level in the past decade

821   by ~0.76 μmol kg^{-1} for 100 – 600 m average and ~0.82 μmol kg^{-1} for 0 – 2000 m average within

822   2015-2023 (**Fig. 24**).

823   By means of these tests we demonstrate that QC and bias adjustment can impact the estimation

824   of the oxygen changes at various temporal-spatial scales, highlighting the need for careful oxygen

825   data processing before application. However, we note here that the validity of the mapping

826   approach on oxygen reconstruction has not been thoroughly evaluated, which deserves a separate

827   study.
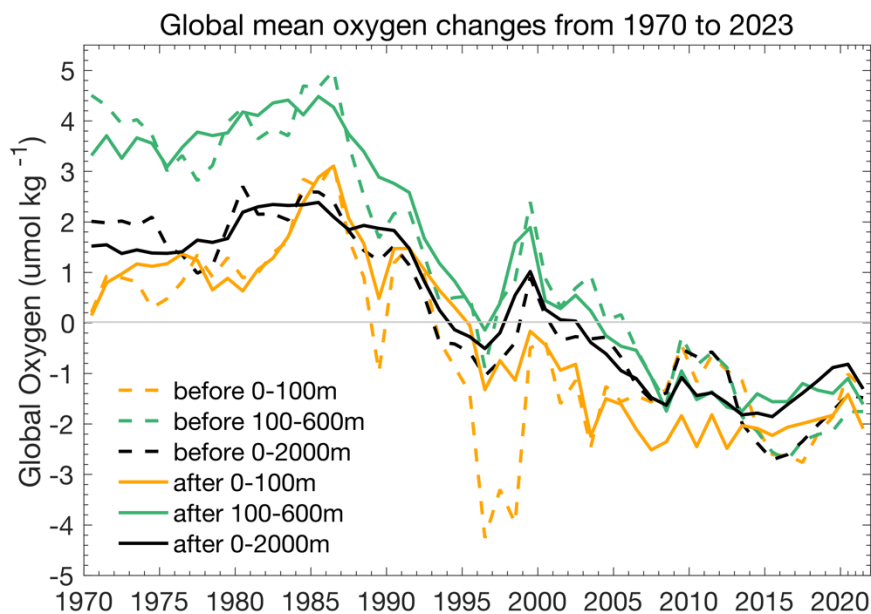
828

829   **Figure 24. The reconstructed global averaged oxygen time series before (dashed line) and**

830   **after (solid line) QC/adjustment from 1970 to 2023 for the layers 0 – 100 m,   100 – 600 m and**

831 **0 – 2000 m. Here, we combine each successive three years of data to estimate the oxygen**

832 **changes. The anomalies are calculated relative to the climatology shown in Fig. 23.**

833

834 **8   Conclusion and Discussion**

835   This study developed a new automated QC scheme for ocean oxygen profile data and applied it

836 to the OSD and CTD oxygen profiles from the WOD and to the Argo float oxygen profiles provided

837 by national DACs. The procedure consists of ten quality checks based on local or global parameter

838 thresholds. Some checks are conceptually similar to the quality checks used to validate the profiles

839 in the World Ocean Database (Boyer et al., 2018) (for example, the global range test and vertical

840 gradient test) and in the Argo data acquisition centers (Thierry et al., 2021) (for example, spike and

841 "frozen" profile tests). Howevert we provide additional checks (for example, test for the number of

842 local extrema and local climatological range test) which increase the ability of the QC procedure to

843 better identify erroneous data. For instance, the procedure proves whether an oxygen value falls out

844 of accepted ranges (defined by globally or locally) or whether an oxygen profile exhibits a very

845 untypical shape. The shape of the profile is characterized by the vertical oxygen gradient, the

846 number and magnitude of local oxygen extrema, and by the presence of spikes. The check is also

847 done for the so-called "frozen" profiles occurring when the oxygen sensor stucks and reports the

848 same values throughout the profile.

849   The QC procedure presented here is tailored for the quality assessment of the archived oxygen

850 data obtained both by Winkler methods and sensors. Large ocean depositories like WOD often

851 contain observed data that have already undergone a certain degree of QC and adjustment.

852 Therefore, our QC procedure differs from the real-time QC of dissolved oxygen observations by

853 means of oxygen sensors as suggested in the frame of the Integrated Ocean Observing System

854 (IOOS) in the quality control manual by Bushnell et al. (2015) (B2015 hereafter). Three quality

855 tests which have been required or suggested in that manual can be applied only to the real time data:

856 the application of the gap test needs the time stamp of each measurement, the application of the

857 syntax test requires the full original data record, and the application of the neighbor test is possible

858 only in the case when a nearby second sensor is installed on the device. Information needed for

859 these tests is not kept in the WOD therefore these tests cannot be applied to "static" archive data.

860 Five other tests outlined in B2015 are conceptually similar to the tests applied by our QC procedure:

861 location test, gross range test, climatology test (all three required by B2015), spike test and flat line

862 test (both recommended by B2015). In a deviation from our QC procedure, thresholds for test

863   variables according to B2015 should be chosen subjectively by operators in the data centers. We

864   note that the metadata on decisions made operators are usually missing in the data archives.

865   The novelty of the proposed quality scheme is that the threshold choice is based on the

866   respective statistics of test variables, and the Gaussian distribution is not assumed for the important

867   local climatological range checks for oxygen and for oxygen vertical gradient. The QC procedure

868   presented in this study was benchmarked against several hydrographic datasets known for their

869   outstanding measurement quality, with WOCE experiment data collection being the largest and best

870   documented. Analysis of the outliers and their distribution among distinct hydrographic sections

871   and cruises suggests the ability of the procedure to flag outliers but retain the overwhelming

872   majority of good data. The accompanying diagnostic tool provides the overview of outlier scores

873   and permits tuning of thresholds when new benchmark quality-controlled datasets become

874   available. Finally, we note that the transparent choice of test threshold values on the basis of the

875   underlying statistics and the subsequent analysis of outliers for each quality check permits further

876   tuning of the quality control procedure in order to increase the percentage of true outliers and to

877   decrease the percentage of falsely identified outliers.

878   Further, we estimated possible residual oxygen biases in the delayed-mode adjusted Argo

879   oxygen profiles. The bias estimates are based on the collocated Argo and discrete water sample

880   ship-based profiles. The latter represents reference measurements as the bottle samples are analyzed

881   by means of the Winkler chemical method. The size of the collocation bubble (e.g., the maximum

882   distance between two profiles and the maximum time difference) was set at 100 km and 5 years,

883   respectively, after several experiments with different bubble sizes. Residual biases relative to the

884   Winkler reference data are represented by the difference at an isobaric level between the Argo

885   sensor oxygen value and the Winkler oxygen, with the overall bias at each level being defined by

886   the average of individual differences. To reduce the impact of time- and spatial variability, the final

887   bias assessment is done for the layer 1000-1900m, which is typically located below the main

888   thermocline.

889   Using all available Argo profiles which have collocations with reference Winkler data, we

890   calculated overall oxygen offsets for six models of oxygen sensors implemented on Argo BGC

891   floats and for six Argo DACs. Our results suggest that derived biases are both sensor- and DAC-

892   specific, with the electrochemical SBI-series sensors exhibiting a positive bias in the range from 0.5

893   to 2.6 μmol/kg. The optoid sensors typically are characterized by negative biases ranging between -

894   0.7 and -6.2 μmol/kg depending on sensor model and DAC. Only for

895   AANDERAA_OPTODE_3830 small positive offsets were found for AOML and CSIRO, as well as

896   positive offsets for SBE63_OPTODE for Coriolis and CSIRO. This diagnosed biases are crucial to

accurately identify the deoxygenation trend, as current assessments suggest an upper 1000 m O_2 content decrease of 0.2–1.2 µmol kg^{-1} dec^{-1} during 1970–2010 (Gulev et al. 2023). Our calculations suggest that at least 1000 collocation pairs are needed for the stable residual bias estimation. This number of collocations is available only for AOML, Coriolis, JMA, CSIRO, INCOIS, and MEDS datasets.

Diagnosed residual biases for the quality-controlled CTD oxygen sensor profiles revealed a good agreement between the CTD and Winkler reference data, with a small median bias of 0.25 µmol kg^{-1} within the layer below 1000 m. Because of a relatively small bias value, which is well within the uncertainty of the CTD sensors and due to a non-uniform spatial CTD bias pattern, the diagnosed overall bias is not considered to be a common and robust feature, and no adjustment of CTD data is performed in this study. Our preliminary investigation also indicates that the CTD offset varies cruise-by-cruise, probably associated with the differences in the calibration or re-calibration (or post-processing). Therefore, the follow-on work should include investigating the offsets on a cruise-by-cruise basis and providing an understanding of the causes of bias. Only after these examinations are done can the adjustment of CTD profiles be physically tenable.

This study also has some limitations and caveats: (1) Although systematical errors have been identified for Argo oxygen data, the cause of the biases is still poorly known and requires further work. The differences between the DAC centers are also mysterious, and we suspect that the non-standard adjustment procedure developed by different National Argo Data Centers and the difference in sensors on Argo floats used in different countries might be responsible for the differences in diagnosed biases, which needs further confirmation. (2) Because the sources of biases are poorly known, the correction proposed in our study is largely empirical and only applies to the Argo data used in this study. If the Global Argo Data Center updates quality control and adjustment procedures, our bias corrections also require an update. (3) The QC procedure is designed to detect and flag the outliers. However, there are also risks of removing the "real extremes" in the ocean, especially under rapid climate change, as ocean extreme events are expected to become more frequent. One possible way to partly resolve this problem is imposing a trend in the local climatological range, accounting for the time-variation of the local oxygen distributions due to climate change, which would help to reduce the false rejection of the real extreme data. This requires further work when the local oxygen trends become clearer. (4) The Winkler data are used in this study as a reference. However, it is likely that the Winkler data are not always taken to the same standard, thus posing inconsistency within the Winkler dataset, especially for the data taken by different countries and in different time periods. Investigating offsets on a cruise-by-cruise basis is also recommended in the future, as for CTD data.

In summary, this study proposed a new quality control approach and bias assessment for the CTD, bottle, and Argo oxygen data and investigated the consistency between these three primary instrumentation types. Our investigations ensured the consistency between the three datatypes and provided a solid basis for merging them into a single, integrated, and homogeneous oxygen database. Therefore, the database obtained in this study supports the next-step assessment and understanding of the change in ocean oxygen levels.

9   Data availability

The quality control procedure described above was applied to the OSD and CTD oxygen profiles between 1920 and 2023 from the World Ocean Database (https://www.ncei.noaa.gov/access/world-ocean-database-select/dbsearch.html) and to the oxygen profiles from the BGC Argo floats (https://www.seanoe.org/data/00311/42182/). The resulting dataset comprises observed level data with quality flags, and data interpolated on 10-meter levels. The data are in NetCDF format and include metadata information. The complete dataset (Gouretski et al., 2023) can be found at http://dx.doi.org/10.12157/IOCAS.20231208.001 and http://www.ocean.iap.ac.cn/ftp/cheng/IAP_oxygen_profile_dataset

10   Code availability

The code of the QC system developed in this paper is available at http://www.ocean.iap.ac.cn/ftp/cheng/IAP_oxygen_profile_dataset/QC_Code_SAMPLE.zip.

Author contributions.

LC and VG – conceptualization, supervision, methodology; VG – software, formal analysis, data validation, visualization, and writing (original draft preparation, final version, and editing); JD, XX, FC – methodology, data curation; LC – writing, analysis, methodology, funding acquisition; ZT – preparing data, formatting.

Competing interests. The contact author has declared that none of the authors has any competing interests.

Acknowledgements. We are thankful to the colleagues from the National Centers for
Environmental Information (NCEI) and the Argo Global Assembly Center (GDAC) for providing
access to the data used in this study (specific Argo DACs are noted in the text). We also thank two
anonymous reviewers for their detailed and constructive comments. The Argo data were collected
and made freely available by the International Argo Program and the national programs that
contribute to it (ARGO, 2000). The Argo Program is part of the Global Ocean Observing System.

Financial support. This study was supported by the Strategic Priority Research Program of the
Chinese Academy of Sciences [grant number XDB42040402], the National Natural Science
Foundation of China [grant numbers 42122046 and 42076202], and the Youth Innovation
Promotion Association, CAS [grant number 2020-077]. The author also acknowledges the support
from the new Cornerstone Science Foundation through the XPLORER PRIZE, Youth Innovation
Promotion Association, Chinese Academy of Sciences.

References

Adil, I. H. and Irshad, A. R.: A modified approach for detection of outliers, Pak. J. Stat. Oper. Res.,
 XI, 1, 91-102, 2015.

Argo (2024). Argo float data and metadata from Global Data Assembly Centre (Argo GDAC).
 SEANOE. https://doi.org/10.17882/42182.

Bittig, H. C., Maurer, T.L., Plant, J. N., Schmechtig, C., Wong,A. P. S. , Claustre,H., Trull, T. W. ,
 Udaya Bhaskar, T. V., Boss, E., Dall'Olmo, G., Organelli, E., Poteau, A., Johnson, K. S.,
 Hanstein, Leymarie,C., E., Le Reste, S., Riser, S. C., Rupan, A., Taillandier, V., Thierry, V. and
 Xing, X. : A BGC-Argo Guide: Planning, Deployment, Data Handling and Usage, Front. Mar.
 Sci., 6:502, doi: 10.3389/fmars.2019.00502, 2018.

Baranova, O. K., Seidov, D., and Reagan, J. R.: World Ocean Atlas 2018, Volume 3: Dissolved
 Oxygen, Apparent Oxygen Utilization, and Oxygen Saturation. A. Mishonov Technical Ed.;
 NOAA Atlas NESDIS 83, 38pp, 2018.

Breitburg, D. et al. Declining oxygen in the global ocean and coastal waters. Science 359,
 eaam7240 (2018).

Bittig, H. C., and Körtzinger, A. (2015). Tackling oxygen optode drift: Near-surface and in-air
 oxygen optode measurements on a float provide an accurate in situ reference. *J. Atmos. Ocean.
 Technol.* 32, 1536–1543. doi: 10.1175/JTECH-D- 14- 00162.1

993   Boyer, T. P., Baranova, O.K., Coleman, C., Garcia, H. E., Grodsky, A., Locarnini, R. A., Mishonov,
994   A. V., Paver, C. R., Reagan, J. R. , Seidov, D., Smolyar, I. V., Weathers, K., Zweng, M.M.:
995   World Ocean Database 2018, A. V. Mishonov, Technical Editor, NOAA Atlas NESDIS 87,
996   2018.

997   Bushnell, M., R. Toll., and H. Worthington: Manual for real-time quality control of dissolved
998   oxygen observations: a guide to quality control and quality assurance for dissolved oxygen
999   observations in coastal oceans, Integrated Ocean Observing System (U.S.), DOI :
1000   http://doi.org/10.7289/V5ZW1J4J, 2015.

1001 Carpenter, J. H.: The accuracy of the Winkler method for dissolved oxygen analysis, Limnology and
1002   Oceanography, 10, 1, p. 135-140. https://doi.org/10.3419/lo.1965.10.1.0135, 1965.

1003 Cheng, L. J., Zhu, J., Cowley, R., Boyer, T. and Wijffels, S.: Time, probe type and temperature
1004   variable bias corrections to historical expendable bathythermograph observations, J. Atmos.
1005   Ocean. Technol.,31, 1793–1825, doi:10.1175/JTECH-D-13-00197.1, 2014.

1006 Cheng, L., et al. Improved estimates of ocean heat content from 1960-2015. *Sci. Adv*. **3**, 3,
1007   e1601545, https://doi.org/advances.sciencemag.org/content/3/3/e1601545, 2017.

1008 Cheng, L., Trenberth, K. E., Gruber, N., Abraham, J. P., Fasullo, J. T., Li, G., Mann, M. E., Zhao,
1009   X., and Zhu, J.: Improved Estimates of Changes in Upper Ocean Salinity and the Hydrological
1010   Cycle. J. Climate, 33, 10357-10381, https://doi.org/10.1175/JCLI-D-20-0366.1, 2020.

1011 Clark, L. C.: Cellophane/Platinum electrode for blood PO2, J. Appl. Physiology, 6, 189, 1953.

1012 Claustre, H., Johnson, K. S., and Takeshita, Y.: Observing the global ocean with biogeochemical-
1013   Argo, Annual Review of Marine Science, 12, 23–48, 2020.

1014 Coppola, L., Salvetat, F., Delauney, L., Machoczek, D., Larstensen, J., Sparnocchia, S.,Thierry, V.,
1015   Hydes, D., Haller, M.,Nair, R., Lefevre, D.: White paper on dissolved oxygen measurements:
1016   scientific needs and sensors accuracy, 22 pages, 2013.

1017 Cowley, R., Killick, R. E., Boyer, T., Gouretski, V., Reseghetti, F., Kizu, S., Palmer, M. D., Cheng,
1018   L., Storto, A., Le Menn, M., Simoncelli, S., Macdonald, A. M., and Domingues, C. M.:
1019   International Quality-Controlled Ocean Database (IQuOD) v0.1: The Temperature Uncertainty
1020   Specification, Front. Mar. Sci. 8:689695. doi: 10.3389/fmars.2021.6896, 2021

1021 Craig, H.: The GEOSECS program: 1972-1973: Earth Planetary Science Letters, v 23, p 63–64.,
1022   1974

1023 Falck, E. and Olsen, A.: Nordic Seas dissolved oxygen data in CARINA, Earth Syst. Sci. Data, 2,
1024   123–131, https://doi.org/10.5194/essd-2-123-2010, 2010.

1025 Baranova, O. K., Seidov, D., and Reagan, J. R.: World Ocean Atlas 2018, Volume 3: Dissolved

1026   Oxygen, Apparent Oxygen Utilization, and Oxygen Saturation. A. Mishonov Technical Ed.;

1027   NOAA Atlas NESDIS 83, 38pp, 2018.

1028 Deutsch, C., Brix, H., Ito, T., Frenzel, H. & Thomson, L. Climate-forced variability of ocean

1029   hypoxia. *Science* **333**, 336–339, 2011.

1030 Golterman, H. L. The Winkler Determination. In: Gnaiger, E., Forstner, H. (eds) Polarographic

1031   Oxygen ensors. Springer, Berlin, Heidelberg. https://doi.org/10.1007/978-3-642-81863-9_31,

1032   pp.346-351, 1983.

1033 Garcia H. E., Z. Wang, C. Bouchard, S. L. Cross, C.R. Paver, J. R. Reagan, T. P. Boyer, R. A.

1034   Locarnini, A.V. Mishonov, O. K. Baranova, D. Seidov, and D. Dukhovskoy. World Ocean

1035   Atlas 2023, Volume 3: Dissolved Oxygen, Apparent Oxygen Utilization, Dissolved Oxygen

1036   Saturation, and 30-year Climate Normal. A. Mishonov Technical Editor. *NOAA Atlas NESDIS*

1037   *91*, 100 pp. https://doi.org/10.25923/rb67-ns53 , 2024

1038 Good., S., Mills, B., Boyer T., Bringas, F., Castelão, G., Cowley, R., Goni, G., Gouretski, V. and

1039   Domingues, C. M.: Benchmarking of automatic quality control checks for ocean temperature

1040   profiles and recommendations for optimal sets, Front. Mar. Sci., DOI

1041   10.3389/fmars.2022.1075510, 2022.

1042 Gulev, S. et al. Changing state of the climate system. In climate change 2021: The physical science

1043   basis. Contribution of working group I to the sixth assessment report of the intergovernmental

1044   panel on climate change (eds Masson-Delmotte, V. et al.). (Cambridge Univ. Press, 2021).

1045 Gruber, N., Doney, S. C., Emerson, S. R., Gilbert, D., Kobayashi, T., Körtzinger, A., et al.. "Adding

1046   oxygen to argo: Developing a global in situ observatory for ocean deoxygenation and

1047   biogeochemistry," in *Proceedings of Ocean Obs '09: Sustained Ocean Observations and*

1048   *Information for Society*, eds J. Hall, D. E. Harrison, and D. Stammer (New Zealand: ESA

1049   Publication), 12. doi: 10.5270/ OceanObs09.cwp.39, 2010.

1050 Garcia H. E., Z. Wang, C. Bouchard, S.L. Cross, C.R. Paver, J.R. Reagan, T.P. Boyer, R.A.

1051   Locarnini, A.V. Mishonov, O.K. Baranova, D. Seidov, and D. Dukhovskoy. World Ocean

1052   Atlas 2023, Volume 3: Dissolved Oxygen, Apparent Oxygen Utilization, Dissolved Oxygen

1053   Saturation, and 30-year Climate Normal. A. Mishonov Technical Editor. *NOAA Atlas NESDIS*

1054   *91*, 100 pp. https://doi.org/10.25923/rb67-ns53, 2024

1055 Gruber, N. Warming up, turning sour, losing breath: ocean biogeochemistry under global change.

1056   Phil. Trans. R. Soc. A 369, 1980–1996, (2011.

1057 Gouretski, V., Cheng, L., Du, J., Xing, X., Chai, F.: A quality-controlled and bias-adjusted global
1058   ocean oxygen profile dataset, Marine Science Data Center of the Chinese Academy of
1059   Sciences, http://dx.doi.org/10.12157/IOCAS.20231208.001, 2024.

1060 Gouretski, V.: World Ocean Circulation Experiment – Argo Global Hydrographic Climatology,
1061   Ocean Sci., 14, 1127-1146, https://doi.org/10.5194/os-14-1127-2018, 2018.

1062 Gouretski, V. and Reseghetti, F.: On depth and temperature biases in bathythermograph data:
1063   development of a new correction scheme based on analysis of a global database, Deep-Sea
1064   Res., I, 57, 812-833, 2010.

1065 Gouretski, V. V., and Jancke, K.: Systematic errors as the cause for an apparent deep water property
1066   variability: global analysis of the WOCE and historical hydrographic data., Prog. Oceanogr.,
1067   48, 4, 337-402, 2000.

1068 Gregoire, M. et al.: A Global Ocean Oxygen Database and Atlas for Assessing and Predicting
1069   Deoxygenation and Ocean Health in the Open and Coastal Ocean, Front. Mar. Sci., 8, 1-29,
1070   https://doi.org/10.3389/fmars.2021.724913 , 2021.

1071 Helm, K. P., Bindoff, N. L. & Church, J. A. Observed decreases in oxygen content of the global
1072   ocean. *Geophys. Res. Lett.* **38**, L23602, 2011.

1073 Hood, E.M., Sabine, C.L., and M. Sloyan, B.M., eds.:The GO-SHIP Repeat Hydrography Manual:
1074   A Collection of Expert Reports and Guidelines, IPCC Report Number 14, ICPO Publication
1075   Series Number 134, 2010.

1076 Hubert, M. and Vandervieren, E.: An Adjusted boxplot for skewed distributions, Comput. Stat.
1077   Data Anal., 52, 5186–5201, 2008.

1078 Keeling, R.F., Koetzinger, A., and Gruber, N.: Ocean Deoxygenation in a Warming world, Annu.
1079   Rev. Mar. Sci., 2, 199-229. doi:10.1146/annurev.marine.010908.163855, 2010.

1080 Koertzinger, A., Schimanski, J., and Send, U.: High quality oxygen measurements from profiling
1081   floats: A promising new technique, J. Atmos. Ocean. Technol., 22, 302-308, 2005.

1082 Ito, T., Minobe, A., Long, M. C. & Deutsch, C. Upper ocean O_2 trends: 1958–2015. *Geophys. Res.*
1083   *Lett.* **44**, 4214–4223, 2017.

1084 Langdon, C.: Determination of Dissolved Oxygen in Seaweater By Winkler Titration using
1085   Amperometric Technique, The GO-SHIP Repeat Hydrography Manual: A Collection of Expert
1086   Reports and Guidelines, Version 1, (eds Hood, E.M., C.L. Sabine, and B.M. Sloyan), 18pp..
1087   (IOCCP Report Number 14; ICPO Publication Series Number 134), DOI:
1088   https://doi.org/10.25607/OBP-1350, 2010.

1089 Larqué, L., Maamaatuaiahutapu, K., Garçon, V.: On the intermediate and deep water flows in the
1090   South Atlantic Ocean. Journal of Geophysical Research, 102,C6,
1091   https://doi.org/10.1029/97JC00629, 1997.

1092 Long, M. C., Deutsch, C. & Ito, T. Finding forced trends in oceanic oxygen. Global Biogeochem.
1093   Cycles **30**, 381–397, 2016.

1094 Levin, L. A. Manifestation, drivers, and emergence of open ocean deoxygenation. Annu. Rev. Mar.
1095   Sci **10**, 229–260 ,2018.

1096 Johnson, K. S., Plant, J., Coletti, L., Jannasch, H., Sakamoto, C., Riser, S., et al.. Biogeochemical
1097   sensor performance in the SOCCOM profiling float array. J. Geophys. Res. Oceans 122, 6416–
1098   6436. doi: 10.1002/2017JC01283, 2017

1099 Marks, R.: Dissolved oxygen supersaturation and its impact on bubble formation in the southern
1100   Baltic Sea, Hydrol. Res., 39,3, 229-236, 2008.Monhor, D. and Takemoto, S.: Understanding
1101   the concept of outlier and its relevance to the assessment of data quality: Probabilistic
1102   background theory, Earth Planets Space, 57, 1009–1018, 2005.

1103 Oschlies, A. et al. Patterns of deoxygenation - sensitivity to natural and anthropogenic drivers. *Phil.*
1104   *Trans. Roy. Soc. A* **375**, 20160325, 2017.

1105 Praetorius, S. K. et al. North Pacific deglacial hypoxic events linked to abrupt ocean
1106   warming. *Nature* **527**, 362–366, 2015.

1107 Pitcher, G. C., Aguirre, A., Breitburg, D., Cardich, J., Carstensen, J., Conley, D. J., et al. System
1108   controls of coastal and open ocean oxygen depletion. Prog. Oceanogr. 197:102613. doi:
1109   10.1016/j.pocean.2021.102613, 2021.

1110 Roemmich, D., Alford, M. H., Claustre, H., Johnson, K., King, B., Moum, J., et al. On the future of
1111   Argo: An enhanced global array of physical and biogeochemical sensing floats. Front. Mar. Sci.
1112   6:439. . doi: 10.3389/fmars.2019. 00439, 2019.

1113 Saout, C., Ganachaud, A., Maes, C., Finot, L, Jamet, L., Baurand, F., and Grilet, J. Calibration of
1114   CTD oxygen data collected in the Coral Sea during the 2012 Bifurcation cruise. Mercator
1115   Ocean-Coriolis Qarterly Nesletter – Special Issue, #52-May, 34-38, 2015.

1116 Sarachik, E.S.: CLIVAR: A Study of Climate Variability and Predictability: Science Plan. World
1117   Climate Research Programme Report 89, WMO Technical Document No 690. 157 pp, 1995.

1118 Stramma, L., Oschlies, A., and Schmidtko, S.: Mismatch between observed and modeled trends in
1119   dissolved upper-ocean oxygen over the last 50 yr, Biogeosciences, 9, 4045–4057,
1120   https://doi.org/10.5194/bg-9-4045-2012, 2012.

1121 Schmidtko, S., Stramma, L. & Visbeck, M. Decline in global oceanic oxygen content during the
1122   past five decades. *Nature* **542**, 335–339, 2017.

Taillander, V., Wagener, T., D'Ortenzio, F., Mayot, N., Legoff, Ras, H. J., Coppola, L., De
    Fommervault, O. P.,   Schmechtig, C., Diamond, E., Bittig, H., Lefevre, D., Leymarie, E.,
    Poteau, A., and Prieur A.: Hydrography and biogeochemistry dedicated to the Mediterranean
    BGC-Argo network during a cruise with RV Tethys 2 in   May 2015, Earth Syst. Sci. Data,
    10, 627-641, 2018, https://doi.org/10.5194/essd-10-627-2018, 2018.

Takeshita, Y., Martz, O. P., Johnson, K. S., Plant, J. N., Gilbert, D., Riser, S. C., Neil, C., and
    Tilbrook, B.: A   climatology-based quality control procedure for plotting float oxygen data, J.
    Geoph, Res: Oceans, 118, 1-11, doi:10.1002/jgr.20399, 2013.

Tan, Z., Cheng, L., Gouretski, V., Zhang, B., Wang, Y., Li, F., Liu, Z., Zhu, J.: A new automatic
    quality control system for ocean profile observations and impact on ocean warming estimate,
    Deep-Sea Res. Part I: Oceanographic Research Papers, 194,
    https://doi.org/10.1016/j.dsr.2022.103961, 2023.

Tengberg, A., Hovdenes, J., Andersson, H. J., Brocandel, O., Diaz, R., Hebert, D., Arnerich, T.,
    Huber, C ., Körtzinger, A., Khripounoff, A., Rey, F., Rönning, C., Schimanski, J., Sommer, S.
    and Stangelmayer, A. : (2006): Evaluation of a lifetime-based optode to measure oxygen in
    aquatic systems. Limnol. Oceanogr.: Methods, 4, 7-17, 2006.

Thierry, V., Bittig, H., and the Argo-BGC team: Argo quality control manual for dissolved oxygen
    concentration, Version 2.1, Argo Data Management, doi: https://dx.doi.org/10.13155/46542,
    2021.

Tukey, J. W. Exploratory Data Analysis, ed. Pierson, ISBN-10: 0201076160, 503 pp., 1977.

Uchida, H., Johnson, G. C., and McTaggart, K. E.: CTD Oxygen sensor calibration procedures. The
    Go-SHIP Hydrography Manual: A Collection of Expert Reports and Guidelines. IOCCP Report
    No. 14, ICPO Publication Series No. 134, Version 1, 17p., 2010.

WHPO: WOCE Operations Manual, Section 3.1.3: WHP operations and methods, WOCE report no.
    69/91, WHPO 91-1. 80 pp., 1991.

Winkler, L.: Die Bestimmung des in Wasser gelosten Sauerstoffes. Berichte der Deutschen
    Chemischen Gesellschaft. 21 (2): 2843–2855. doi:10.1002/cber.188802102122, 1888.

Wunsch, C.: Towards the World Ocean Circulation Experiment and a bit of aftermath, Springer-
    Verlag, Jochum, M., Murtugudde, R., Phys. Oceanogr., 181-201, 2006.

Yang, J., Rahardja, S., and Fränti, P.: Outlier Detection: How to Threshold Outlier Scores?,
    AIIPCC '19: Proceedings of the International Conference on Artificial Intelligence, Information
    Processing and Cloud Computing, December 2019. Article No.: 37, p. 1–6
    https://doi.org/10.1145/3371425.3371427, 2019.